UNLIMITED DISTRIBUTION

National Defence
Research and Development Branch

Défense nationale
Bureau de recherche et développement

TECHNICAL MEMORANDUM 92/215
June 1992

ACOUSTIC PROPAGATION LOSS PREDICTIONS FOR A SITE ON THE BERMUDA RISE AT LOW AND VERY LOW FREQUENCIES

Frederick D. Cotaras - James A. Theriault

Defence Research Establishment Atlantic

Centre de Recherches pour la Défense Atlantique

DEFENCE RESEARCH ESTABLISHMENT ATLANTIC

9 GROVE STREET
P O BOX 1012
DARTMOUTH, N S
B2Y 3Z7

TELEPHONE
(902) 426 3100

CENTRE DE RECHERCHES POUR LA DÉFENSE ATLANTIQUE

9 GROVE STREET
C P 1012
DARTMOUTH N E
B2Y 3Z7

UNLIMITED DISTRIBUTION

National Defence
Research and Development Branch

Défense nationale
Bureau de recherche et développement

ACOUSTIC PROPAGATION LOSS PREDICTIONS FOR A SITE ON THE BERMUDA RISE AT LOW AND VERY LOW FREQUENCIES

Frederick D. Cotaras - James A. Theriault

June 1992

Approved by C.W. Bright
Director / Sonar Division

Distribution Approved by C.W. Bright

C.W. Bright
Director / Sonar Division

TECHNICAL MEMORANDUM 92/215

Defence Research Establishment Atlantic

Centre de Recherches pour la Défense Atlantique

Canada

Abstract

Low (10–100 Hz) and very low (1–10 Hz) frequency acoustic propagation loss is predicted for a site on the Bermuda Rise near 30°N 69°W. An extensive survey of the open literature is reported, and a geo-acoustic model of the acoustic environment at the site is developed. The results of a brief numerical investigation of the effect of shear waves and detailed sub-bottom layering on the acoustic propagation-loss predictions are discussed. The acoustic propagation-loss model used is SAFARI, which accounts for shear waves in the sediment but assumes a range-invariant environment. The propagation-loss predictions for 5, 10, 20, and 50 Hz are then presented. Also presented are predictions of the reflection loss in the form of grey-scale plots as a function of frequency and grazing angle. No comparison with experimental data is attempted.

Résumé

On prédit les pertes de propagation acoustique en basses fréquences (10 – 100 Hz) et en très basses fréquences (1–10 Hz) pour un emplacement sur la montée des Bermudes, aux environs de 30° de latitude nord et de 69° de longitude ouest. Un dépouillement exhaustif de la littérature courante du domaine a été réalisé et un modèle géacoustique de l'environnement acoustique de l'emplacement a été développé. Le document décrit les résultats d'une brève étude numérique de l'effet des ondes de cisaillement et de la formation détaillée de couches dans le sous-sol marin sur les prédictions des pertes de propagation acoustique. On utilise le modèle des pertes de propagation acoustique SAFARI, qui tient compte de l'effet des ondes de cisaillement dans les sédiments, mais suppose un environnement à portée invariante. On présente ensuite les prédictions des pertes de propagation à 5, 10, 20 et 50 Hz. On présente aussi les prédictions de la perte en réflexion sous forme de graphiques à échelle de gris, ainsi qu'en fonction de la fréquence et de l'angle rasant. On n'a tenté aucune comparaison avec les données expérimentales.

Contents

List of Figures

1 Introduction

The purpose of this document is to provide predictions of the acoustic propagation loss for a site in the North Atlantic Ocean for low (10–100 Hz) and very low (1–10 Hz) frequencies. The work was performed to support signal-processing experiments carried out by DREA in 1991 within a 180 km circle centred at 30°N 69°W, which is on the southwestern part of the Bermuda Rise. Because no acoustic propagation-loss data are available to compare to our predictions, we rely entirely on the predictions provided by a computer propagation-loss model. The accuracy of the predictions from a computer model is limited by the accuracy of its input, the geo-acoustic model. Accordingly, a considerable portion of this paper is centred on the derivation of our geo-acoustic model. Also provided in this document are estimates of the reflection loss (plane-wave reflection coefficient in dB) as a function of grazing angle and frequency. The results of a numerical investigation of the effect of both shear waves and sub-bottom layering in deep-ocean sediments on the propagation-loss predictions are also presented.

The document is structured as follows. The next section is an overview of how the computer propagation-loss model was selected. The motivation for a detailed sub-bottom layering and the procedure used to arrive at the geo-acoustic model for the site are presented in the third section. A limited discussion of the sensitivity of the acoustic propagation-loss predictions to some of the geo-acoustic inputs is provided in the fourth section along with the results of the numerical investigation on the effects of shear waves and the detailed sub-bottom layering on reflection and propagation loss. Presented in the fifth section are the propagation-loss predictions for 5, 10, 20, and 50 Hz sources at depths of 15.2 and 91.4 m and receiver depths of 30.5 and 304.8 m. The final section is a summary of the main results.

2 Choice Of The Acoustic Propagation Model

The deep-ocean sea-bed plays an important role in low frequency acoustic propagation; see, for example, Ref. [1]. Experimental evidence for the importance of the sub-bottom refracted paths and a review of the early literature is given by Christensen, Frank, and Geddes [2]. Experimental evidence of the importance of not only sub-bottom refraction, but also sub-bottom reflection is given by Frisk, Doutt, and Hays [3]; the unpublished results of several DREA experiments indicate similar phenomena [4]. Thus, the chosen acoustic propagation-loss model should account for not only water-borne paths, but also sub-bottom reflected and refracted paths.

The coupling of acoustic waves into shear waves has been observed in shallow-water environments; see, for example, Ref. [5]. Although similar coupling is not widely discussed as an important propagation-loss mechanism in deep-water environments, the possibility exists. It has been known for some time that when a compressional plane wave travelling in a fluid half-space strikes a plane interface with a solid half-space, both a shear and a compressional wave are excited in the second half-space. Furthermore, under certain conditions, waves at the fluid-solid interface are excited [6]. It is also well known that, in ocean sediments, shear waves are attenuated at a much greater rate (in dB/wavelength) than compressional waves [7]. The chosen acoustic propagation-loss model should, therefore, account for both shear- and compressional-

wave propagation in the ocean bottom. In this way, the effect of shear waves on the propagation loss in this deep-water environment may also be investigated numerically.

The choice of acoustic propagation-loss model is first restricted to models that are available at DREA. The basic choices are ray models, parabolic-approximation models, normal-mode models, and full-wave models. Although able to handle range-dependent environments, ray models are not used because the available ray models treat the bottom using reflection-loss tables. Thus, energy that enters the bottom is assumed to never re-enter the water column, which means that these ray models cannot predict sub-bottom reflection or refraction. Moreover, ray models tend to inaccurately account for the surface interference effect; see, for example, Ref. [8]. Like most ray models, parabolic-equation models handle range-dependent environments. The parabolic-equation models have, however, the advantage of accounting for sub-bottom refraction and, with modifications to the input, sub-bottom reflections [3]. Many parabolic-equation models are, unfortunately, limited to moderate to shallow grazing angles. Moreover, the available parabolic-equation models assume a fluid bottom, that is, they do not account for shear waves in the bottom. A third type of model is based on normal modes. Although two of the available normal-mode models, PROLOS [9] and KRAKEN [10], account for shear waves in the bottom, they are not used because they are computationally too inefficient for these frequencies in this environment. The fourth class of model is the full-wave type, which gives the exact solution to the problem of one-way sound propagation in a layered fluid over a layered solid bottom—if the environment is range independent. For our site, shear effects as well as sub-bottom reflections and refractions are assumed to be more important than the range-dependent effects. We therefore choose the acoustic propagation-loss model called SAFARI, which is a full-wave model [11].

3 Development Of The Geo-acoustic Model

3.1 Introduction

Bowles [12], who gives an extensive list of references to the literature about the Bermuda Rise, describes the Rise as follows: "The Bermuda Rise is an elongate topographic arch (2000 × 1000 km) rising approximately 1 km above the surrounding ocean basin of the North Atlantic." Figure 1 shows the location of our site on the Bermuda Rise and the other general regions of the North Atlantic Ocean [13]. Unfortunately, despite the increasing number of measurements of geo-acoustic properties of the sea-bed, only a small amount of information is available on the geo-acoustic properties of the Bermuda Rise.

In this section an outline of how the estimates of the geo-acoustic properties for our site, which is on the southern edge of the Bermuda Rise near the Hatteras Abyssal Plain at 30°N 69°W, is given. The section is organized as follows: first, the question of the detail required in the geo-acoustic model is addressed. Next, an outline of the approach taken in the development of the geo-acoustic model is given. The remainder of the section discusses how the numbers in the geo-acoustic model are chosen.

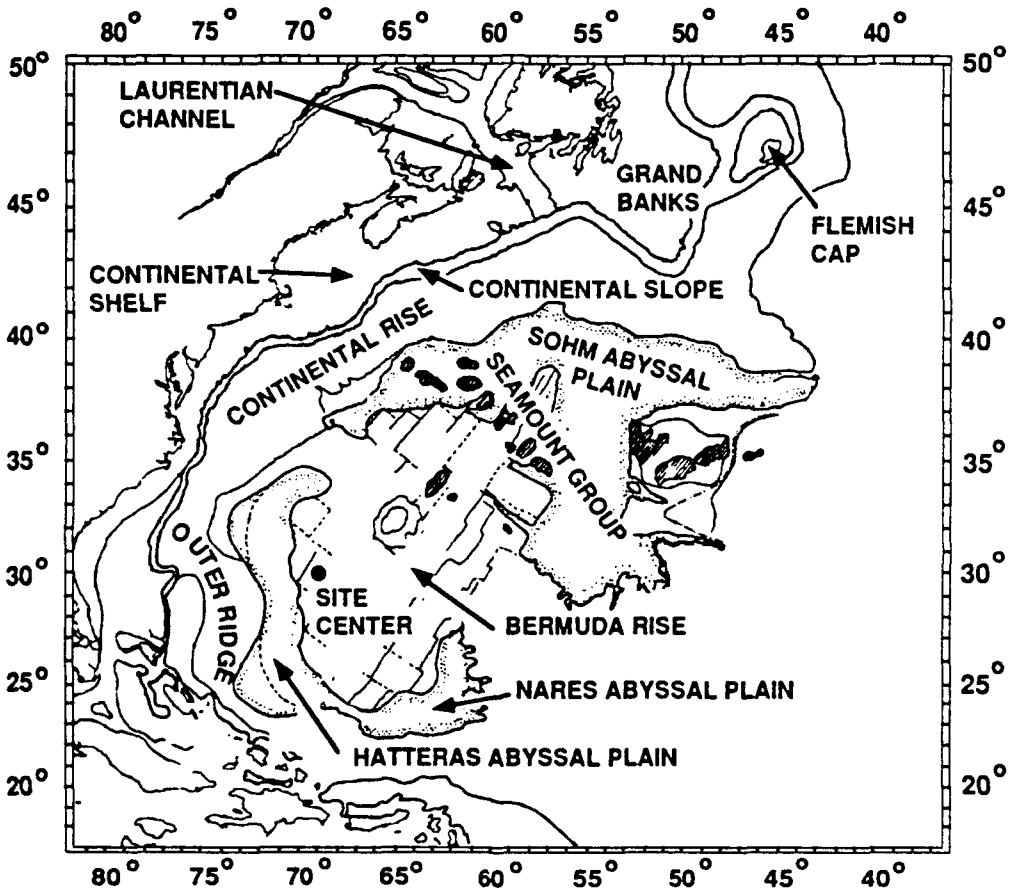

Figure 1: *Map showing locations of the major deep-water regions of the North Atlantic Ocean. After Plate 20 in Ref [13].*

3.2 How Much Detail?

We now briefly attempt to answer the question posed in the title of this section, namely, how much detail in the geo-acoustic model is sufficient? We start by noting the results of Frisk *et al.*, who successfully modelled acoustic propagation on the Bermuda Rise at 220 Hz [3]. They assumed a 160 m unconsolidated sediment layer with an approximately constant sound-speed gradient over a homogeneous, denser, faster half-space. It turns out, as we see below, that what they called a half-space is in fact a series of reflector layers that overlay hundreds of meters of sediment. Nevertheless, Frisk *et al.*'s relatively simple model gave results that compared well with their measured propagation-loss data. But is such a simple model sufficient for very low frequency propagation? In this document, we show through numerical examples that the simple model does not always work for very low frequencies.

At very low frequencies, the wavelengths are large; for example, the wavelength at 5 Hz is about 300 m. With these wavelengths, the upper unconsolidated sediment layer appears thin, and the structure below will affect the propagation characteristics. If the frequency is increased by an order of magnitude to 50 Hz, the upper unconsolidated layer appears thick relative to a wavelength, and the deeper layers are, consequently, not as important. Accordingly, we argue that, although the need for fine detail decreases with decreasing frequency, the need for information on the geo-acoustic properties of the deeper layers increases.

The need for detailed information on the deeper layers may be reinforced by considering the textbook calculation for the acoustic reflection loss at a single homogeneous layer. Assume that the angle of incidence is constant. If the layer thickness is much greater than a wavelength, then the amplitude of the reflected signal may be calculated without considering the properties of the third medium, that is, the layer may be treated as a half-space. However, if the layer thickness is on the order of a wavelength, then the acoustic properties of the third medium must be considered in order to calculate the amplitude of the reflected signal accurately. Moreover, if the layer thickness as well as the angle of incidence are held constant but the acoustic wavelength, which is on the order of the layer thickness, is varied, then the amplitude of the reflected signal will vary radically from total reflection to perfect transmission. Examples of this variation are shown in Section 4.1 where the reflection loss for our site is examined.

Some additional qualitative analysis adds credence to our requirement for detailed information on the deep-sediment layers in a deep ocean. Aside from the reflection loss, three other physical effects that vary with frequency are (1) attenuation (both shear and compressional), (2) decay of the evanescent waves (defined below), and (3) intensity near caustics in the sub-bottom layers. The attenuation effects are straightforward. The approximately linear frequency dependence of both compressional- and shear-wave attenuation (approximately constant attenuation per wavelength) indicates that lower frequency waves propagate with less attenuation and, accordingly, reach greater depths [7]. The second and third effects are more complicated.

The frequency-dependent contribution of evanescent waves is now examined. Consider two homogeneous fluid half-spaces with a plane interface, and assume that the upper half-space has a sound speed less than that of the lower. If a harmonic plane-wave that is travelling in the upper half-space strikes the interface at an angle such that total internal reflection occurs (i.e., beyond the critical angle), then the wavefield excited in the lower half-space is evanescent: the wavefield in the lower half-space is not propagating, but rather travels along the interface with

an amplitude that decays exponentially with the distance away from the interface *normalized by the wavelength*. If the lower medium is not in fact a true half-space, but a series of layers with finite thicknesses, the problem is much more complicated. Under certain conditions however, it is possible for an evanescent wave to excite a propagating wave in the deeper layers. Because of the nature of the decay of the evanescent wave, the amount of excitation in the deeper layers is frequency dependent. Lower frequency waves excite evanescent waves that decay more slowly (on an absolute scale) and can, therefore, couple more energy into propagating waves in the deeper layers. Thus, the deeper layers may influence propagation at low and very low frequencies.

Another frequency dependent propagation effect is the intensity near a caustic. Consider two fluid half-spaces, the upper being homogeneous and the lower being inhomogeneous with a sound speed that increases linearly with depth. Assume that an incident spherically spreading wave strikes the interface at such an angle that transmission occurs. The transmitted wave refracts upwards and then re-enters the upper half-space. This problem has been previously analyzed and is presented in detail in Section 47 of the book by Brekhovskikh [14]; here only one of the concepts discussed by Brekhovskikh is presented. Brekhovskikh defines a parameter δ that is of the order of the width of the band of the caustic, while $1/\delta$ is proportional to the magnitude of the caustic. Brekhovskikh goes on to show that δ is proportional to a fractional power of the wavelength. Thus, although it is not a linear relationship, the intensity and width of the caustic region vary with the wavelength. At lower frequencies, the caustic region will be lower in intensity and more diffuse in space, whereas at higher frequencies, the caustic region will be higher in intensity and sharper spatially. Consequently, although ray theory would indicate that the propagating energy is confined to the ray tubes and does not enter acoustic shadow zones, the reality is that the energy does spread into shadow zones and that the spatial distribution of this energy is frequency dependent. Thus, the depth to which the sediment should be modelled must increase as the frequency is lowered.

In summary we note that for very low frequency propagation in the deep ocean, the depth to which the geo-acoustic model extends will probably have to greatly exceed that of Frisk *et al.* As the frequency is lowered, the sediment layers appear thinner and the reflection- and propagation-loss calculations become more dependent on the deeper layers. Similarly, the attenuation decreases with frequency, and more sound energy penetrates to the deeper layers. Moreover, the spatial extent of wave phenomena such as caustics and evanescent waves increases, and the phenomena are, accordingly, influenced by deeper layers. The combined effect of all of these factors is assessed in Section 4.1 where the reflection- and propagation-loss predictions with and without detailed information on the deeper layers are compared.

3.3 Overview of our Approach to Geo-acoustic Modelling

As noted earlier, to improve the accuracy of low frequency acoustic propagation-loss predictions, some acoustic propagation-loss models account for both compressional- and shear-wave propagation in the sea-bed. Consequently, these models, of which **SAFARI** is one, require more information on the geo-acoustic properties of the bottom. In addition to the sound speed in the water column, these models require estimates of the density as well as compressional- and shear-wave speeds and attenuations for the sea-bed. Under ideal circumstances, these properties would be known as a function of depth from the sea-bed surface to the depth from which no

sound returns, the acoustic basement.

In a series of review/tutorial type papers, Hamilton establishes a procedure for obtaining estimates of the geo-acoustic properties listed above [15, 16, 17]. In these papers, Hamilton effectively summarizes his earlier papers on each individual property as well as updates his estimates of some geo-acoustic properties [19, 20, 21, 22, 23, 24, 25, 26, 27]. Our approach is to use Hamilton's procedure and to compare his estimates with any other available information. The importance of Hamilton's works to this document cannot be overstated.

A brief overview of Hamilton's procedure is now given. For reasons that will be more apparent later, the geo-acoustic properties of the sea-bed are estimated in the following order: compressional-wave speed, shear-wave speed, density, compressional-wave attenuation, and shear-wave attenuation. The *compressional-wave speed* information is obtained by doing the following:

- Estimate the depth to and sediment type of the sea-bed surface.
- Estimate the sound-speed profile in the water column from historical data.
- Estimate the compressional-wave speed of the sediment at the sea-bed surface and the gradient of the compressional-wave speed in the upper unconsolidated sediment layers.
- Estimate the thicknesses and compressional-wave speeds of the reflector layers that are known to be at the site.

The upper unconsolidated sediment layers are assumed continuous until they reach the first reflector layer, that is, no intermediate sand layers, etc. are assumed. From the first reflector layer down to the acoustic basement, constant sound-speed layers (zero gradient layers) are assumed.

Once the compressional-wave speed profile is complete, estimates of the other properties may be obtained. Estimates of the shear-wave speed are obtained using the compressional-wave speed and the sediment types. Estimates of the density of the sea-bed are obtained using our knowledge of the sediment type to estimate both the density of the sediment at the sea-bed surface and the density gradient with depth. After the first reflector layer is encountered, constant density layers are assumed. An estimate of the compressional-wave attenuation is also obtained from our knowledge of the sediment type. Finally, we estimate the shear-wave attenuation from the compressional-wave attenuation with an upper bound set by the physical requirement that pure dilatation of a solid does not radiate energy.

3.4 Depth to and Sediment Type of the Sea-bed Surface

In support of nuclear waste disposal, several studies of the geotechnical properties of the sea-bed have been undertaken in the Seabed Disposal Program. One site on the Northern Bermuda Rise between 32–36°N and 56–64°W is discussed by Silva *et al.* [28]. Referencing their earlier related studies, Silva *et al.* note that hemipelagic clay covers most of the region to a depth of up to 1000 m. Moreover, they note that the upper 200–300 m of sediment are highly stratified and were deposited at a rate of 40 cm per 1000 years for the past 1.0–1.8 million

years. They also note that the stratified sediments "are primarily illite-rich clays containing a variable calcium carbonate component which fluctuates between 5–37%." Some of their piston core results indicate large variations in the density that are caused by corresponding variations in the water content of the sediment. Although these measurements were not taken at our site, the variations in density are of interest because they might contribute to fluctuations in propagation loss. Because of the lack of detailed information about our site, such variations are not taken into account.

Our estimate of the sediment type is obtained from the study by Embley *et al.* in which 1 m gravity cores were taken [29]. The centre of the Embley *et al.*'s experiment is within our site's boundaries and is indicated in Fig. 2. (Also indicated in Fig. 2 are the locations of boreholes and other geo-acoustic measurements.) Embley *et al.* categorize the sediment as *hemipelagic* silty clays with an average ratio of clay to silt of 4:1. The mean grain size is approximately 1.25–1.5 μm. Based on 45 samples from a variety of ocean regions, Hamilton [15] states that the mean grain size of deep-sea ("red") *pelagic* clay is 1.5 μm and that its composite ratio is 80.9% clay, 19.0% silt, and 0.1% sand. Although Hamilton does not cite values for hemipelagic clay, his pelagic clay values match Embley *et al.* data so well that we assume that the sediment at the surface of the sea-bed is, in Hamilton's terminology, pelagic clay.

Knowledge of the water depth at the site is required. In Plates 5 and 6 of his 1986 work, Tucholke provides estimates of the depths to the acoustic basement (from sea level) and the sediment thicknesses, which at the site are, respectively, about 6200 m and 1000 m [31]. Thus, the water depth is about 5200 m. Our estimate of the water depth is, however, obtained from the detailed study by Embley *et al.* They estimate the water depth to be approximately 5250 ± 20 m, which is in good agreement with the data of Tucholke.

3.5 Sound-Speed Profile

As indicated earlier, the next item required is an estimate of the sound-speed profile and, in particular, the bottom-water sound speed. Historical sound-speed profiles are obtainable from several sources: two such sources are the ICAPS data base [32] and the document by Podeszwa [33]. Because the site is near the edge of the Gulf stream, the sound-speed profiles are reported to be highly variable, and thus the number of possible profiles is high. The relevant sound-speed profiles from the ICAPS data base are profile numbers 9H-Sargasso, 9H-Stream, and 9D. The profile 9D is from the older version of the ICAPS data base, whereas the same location is now represented by two profiles, 9H-Sargasso and 9H-Stream. The profiles of Podeszwa are divided into two parts: the variable upper region and the more stable lower water mass. The relevant lower water mass profile numbers are A16, A17, and A18. The relevant upper water column profiles are numbers A17b and A17d. Of these profiles, the one that corresponds to our site centre is A17d for the upper region with A16 for the lower region.

All profiles over the entire water column are shown together in Fig. 3 with a detail of the upper portion of the water column shown in Fig. 4. Since profile 9H-Stream varies significantly from all other profiles both in the surface region and at great depth, it is not used in our modelling. This does not mean that the profile is wrong, just that it is less likely to occur. For modelling purposes, Podeszwa's profile A17d with A16 is used. Note that, at a depth of 5250 m,

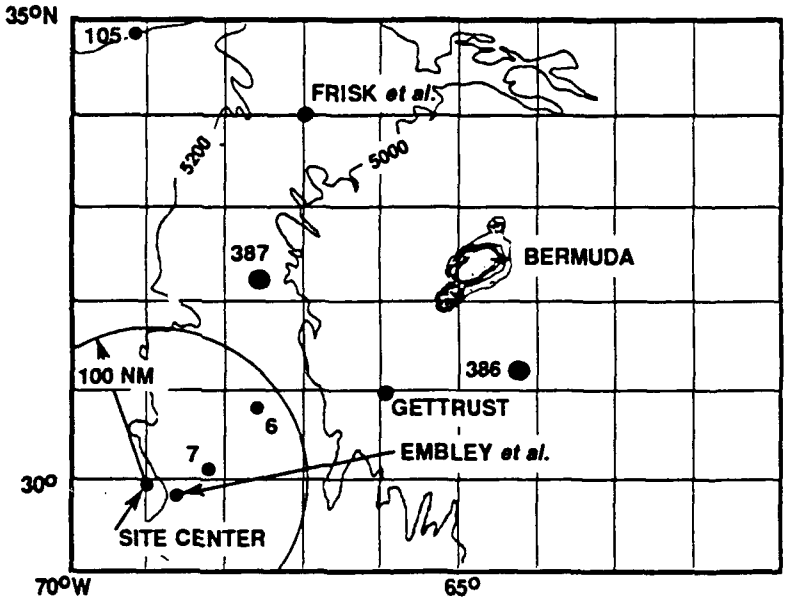

Figure 2: *Map showing locations of the Ocean Drilling Project (ODP) boreholes and seismic profiles in the Bermuda region. After Fig. 1 in Ref. [30].*

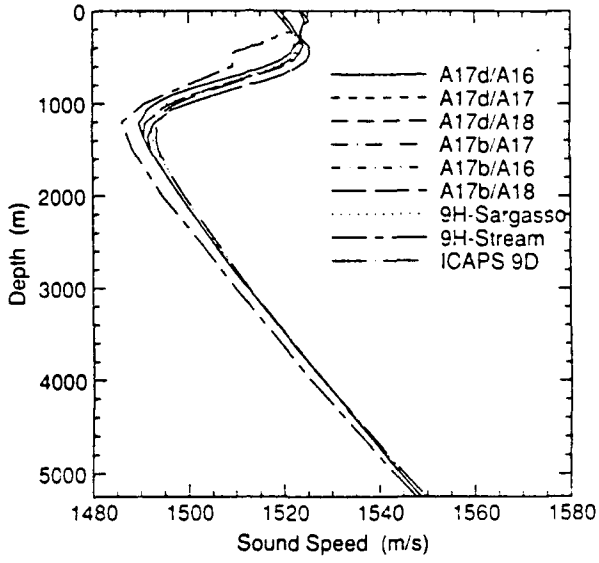

Figure 3: *Historical sound-speed profiles from the ICAPS data base[32] and from the document by Podeszwa [33].*

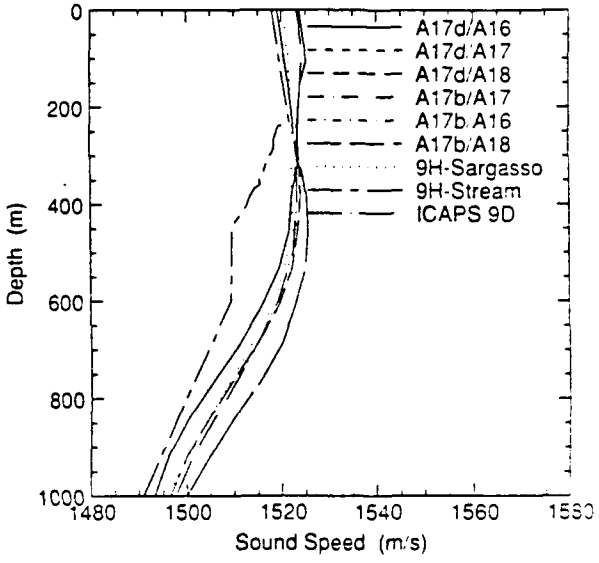

Figure 4: *Detail of upper portion of sound-speed profiles shown in Fig. 3.*

all of Podeszwa's lower water column profiles yield the same sound speed of 1548 m/s. If the actual sound-speed profile is slightly different—which is possible near the Gulf stream, the effect on the propagation loss at very low frequencies is slight. The major effect of a change in the profile is a slight shift in the locations of the convergence zones, which, as we later see, are not large features in very low frequency propagation-loss curves.

3.6 Compressional-Wave Speed of Sediments at the Sea-bed Surface

In lieu of *in situ* measurements, Hamilton recommends that the compressional-wave speed of the surface layer be estimated using the *velocity ratio* for the sediment type at the site. The velocity ratio is the ratio of the compressional-wave speed in the sediment to the sound speed in water when both are at the same temperature, pressure, and salinity. Thus, multiplying the velocity ratio by the bottom-water sound speed yields the sound speed of the sediments at the sea-bed surface. Hamilton's velocity ratio for pelagic clay is 0.976 with a standard error of 0.001 [15]. Multiplying by the bottom-water sound speed leads to a sea-bed surface compressional-wave speed of 1511 m/s. The estimate of the sediment sound-speed at the sea-bed surface is important because it is a key ingredient in the calculation of both the amplitude of the reflected sound and the angle of refraction of the transmitted sound.

3.7 Gradient of the Compressional-Wave Speed in Unconsolidated Sediment

The next item in the development of the geo-acoustic model is to estimate the gradient of the compressional-wave speed. The gradient is important for determining the rate at which sound in the sea-bed refracts and exits the sea-bed. Again, ideally *in situ* measurements would be used: within our site boundaries is Ocean Drilling Project borehole 7 (ODP, formerly Deep Sea Drilling Project) at 31.134°N 68.297°W to a depth of 296 m, and not far away is ODP borehole 6 at 30.840°N 67.648°W (depth 257 m) [34, 35]. Both are indicated in Fig. 2. However, the data from these holes are not sampled continuously in depth. Moreover, Hamilton believes that the ODP data are not suitable for determining the gradients in the top 100 m because of errors in measuring the drilled layer thickness and the sound-travel time [15]. Our estimates of the gradient of the compressional-wave speed are, therefore, obtained using Hamilton's procedure. They are then compared to the results of measurements that were made on the Bermuda Rise site.

Hamilton estimates the sound-speed gradient in pelagic clay to be 1.046/s (based on data from five widely scattered sites) [20]. He also estimates the sound-speed gradient in hemipelagic clay to be 1.151/s (based on four widely scattered sites). With these gradients and our estimate compressional-wave speed of the sediment at the sea-bed surface, an estimate of the compressional-wave speed as a function of depth in the upper unconsolidated layer is at hand. The estimate is now compared with published measurements.

In 1988, Gettrust *et al.* conducted a "high resolution" study of the sediment layer thicknesses and compressional-wave speeds on the Bermuda Rise near 31°N 66°W [36]. The location is shown in Fig. 2, and the corresponding results are shown in Fig. 5 along with the estimates obtained from Hamilton's data. It can be seen in Fig. 5 that the errors in Gettrust *et al.*'s estimates of the compressional-wave speed are moderate to large, whereas the errors in their depth estimates are relatively small. Their data are in reasonable agreement with the gradient of the compressional-wave speed predicted by Hamilton.

Another estimate of the compressional-wave speed as a function of depth is in the 1981 work by Frisk, Doutt, and Hayes, which was performed on the Bermuda Rise at 34° N, 67° W and is indicated on Fig. 2 [3]. By comparing their data (pulsed 220 Hz) with ray and normal-mode model predictions, they infer one estimate of the compressional-wave speed structure. On the other hand, from their parabolic-equation model predictions, they arrive at another only slightly different compressional-wave speed structure. Both of these structures are depicted in Fig. 6 along with the estimates obtained using Hamilton's data. The average slope from their ray and normal-mode modelling is 0.94/s, whereas the estimate from their parabolic-equation modelling is 0.97/s. These slope estimates are in closer agreement with Hamilton's gradient estimate for pelagic clay (1.046/s) than with his gradient estimate for hemipelagic clay (1.151/s).

In a 1980 paper, Houtz defines some sound-speed gradient provinces for the Northwest Atlantic Ocean [37]. (These provinces are the same ones given by plate 6 of the 1986 work by Tucholke [31].) The data do not provide estimates of the sound-speed gradient for the Bermuda Rise; however they do provide an estimate of the average and standard deviation of the compressional-wave speed in the sediment, 2000 m/s and 200 m/s, respectively. Although not indicated on Fig. 2, the province for which these data apply encompasses most of the Bermuda Rise. The data are plotted in Fig. 7, along with the estimates obtained from Hamilton's data.

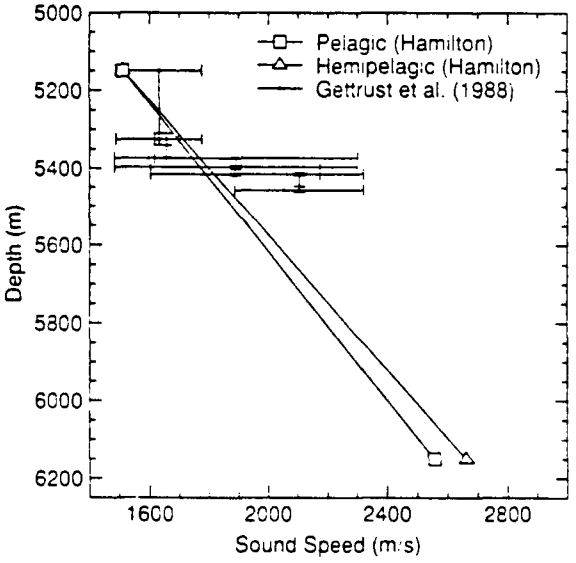

Figure 5: *Compressional-wave speed versus depth for two locations on the Bermuda Rise near 31° N 66° W as found by Gettrust et al. [36].*

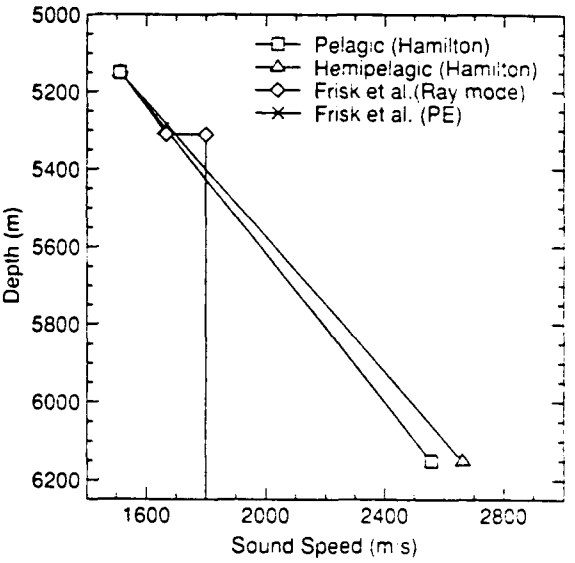

Figure 6: *Compressional-wave speed versus depth estimates used by Frisk, Doutt, and Hayes used in their ray and normal-mode models and parabolic-equation model [3].*

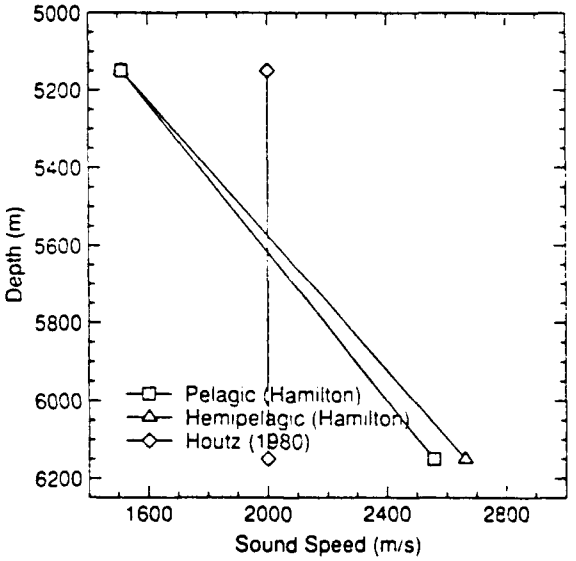

Figure 7: *Compressional-wave speed versus depth for sedimentary province M as defined by Houtz [37].*

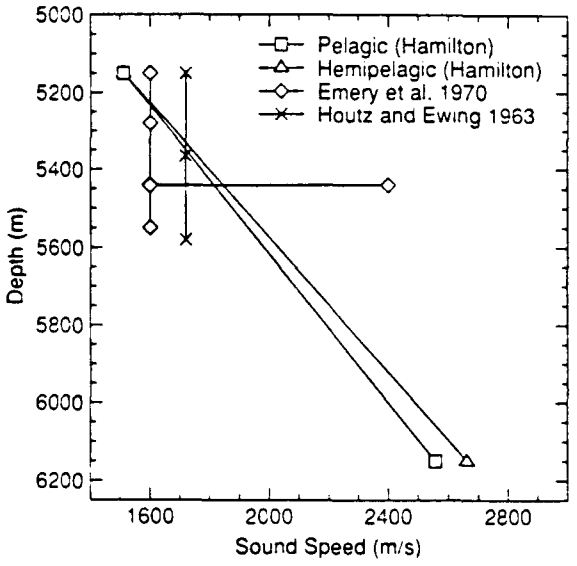

Figure 8: *Geo-acoustic models from Emery et al. [38] and Houtz and Ewing [39] as reported by Frisk, Doutt, and Hayes [3].*

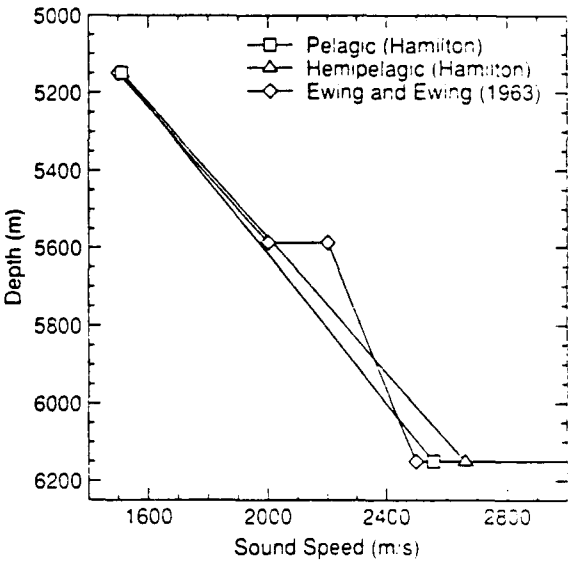

Figure 9: *Compressional-wave speed versus depth for general Bermuda Rise location [40]. Reflector A is shown in Fig. 10*

Houtz's estimate is based on 27 samples and is claimed to be applicable to a maximum depth of 1000 m. Houtz's data appear to be in general agreement with the estimates obtained using Hamilton's data.

General agreement also exists between Hamilton's data and some other early works. Shown in Fig. 8 are Hamilton's data and the data from the 1970 work of Emery *et al.* [38] at 33.483° N, 67.800° W as well as the data from the 1963 work of Houtz and Ewing near 35° N, 67° W [39] (as reported by Frisk, Doutt, and Hayes [3]). In their 1963 discussion of some proposed deep-sea drilling sites, Ewing and Ewing give a summary of their knowledge of a region south-southeast of Bermuda [40]. They provide an estimate of the compressional-wave speed structure in the sediment, which is plotted in Fig. 9.

In summary, the estimates obtained using the procedure set forth by Hamilton are in agreement with all known data. The slope estimates of Frisk, Doutt, and Hayes appear to be the most reliable data and are in closer agreement with Hamilton's gradient estimate for pelagic clay than with his estimate for hemipelagic clay. The pelagic clay gradient estimate from Hamilton is, therefore, used for the initial layer. The depth to which the gradient estimate is valid is addressed in the next section.

3.8 Reflector Layer Thicknesses and Compressional-Wave Speeds

It has been known for some time that the Bermuda Rise has a number of different underlying reflector layers, and the depths of the reflector layers are known to vary with position. As an example of the variability, consider the seismic reflection profile shown in Fig. 10, which is

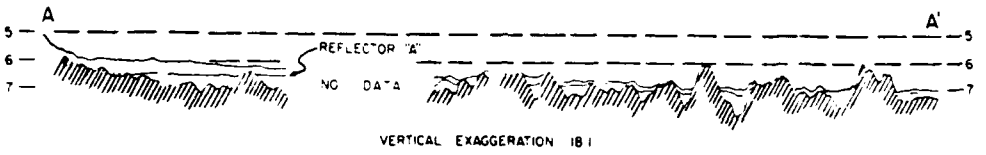

Figure 10: *Reflection profile running approximately south from Bermuda. Vertical axis is reflection time in seconds. Taken from Fig. 2 in Ref. [40].*

taken from Ewing and Ewing's 1963 discussion of some proposed deep-sea drilling sites [40]. The profile runs south from Bermuda and is not over our site, but gives some idea of the rates of change of the reflector layers on the Bermuda Rise. Ewing and Ewing named the reflector "Reflector A". The hashed area in Fig. 10 represents scattering from within layers. The most recent description of the reflector layers on the Bermuda Rise of which we are aware is given by Tucholke [30]. Tucholke indicates that "Reflector A" is not a single reflector, but a considerably more complicated structure that consists of a series of closely spaced discrete layers. Tucholke discusses the origins of the reflector layers at some length.

The depths, thickness, sound speeds, etc. of the layers under our site are required as inputs to the propagation-loss models. Some data are available from the ODP boreholes on the Bermuda Rise. As previously noted, the information from boreholes 6 and 7 is, unfortunately, not useful because the data are too sparsely sampled in depth [35, 34]. The next closest ODP borehole is number 387 at 32.320°N 67.667°W, which is also indicated in Fig. 2 [41]. The data from this borehole are almost continuous in depth, and, for this reason, the ODP borehole 387 data is used.

The compressional-wave speed profile shown in Fig. 11 is obtained through an examination of both the compressional-wave speed data and the discussions of the sediment types in the site report for Borehole 387. Starting at a water depth of 5250 m, the sediment analysis in the site report indicates that the initial 40–98 m are hemipelagic sediments, whereas the sediment is pelagic until about 175 m depth. This layering is ignored because (1) the initial layer depth is not accurately known, and (2) our site's layering could be quite different. (Recall the data are not actually taken at our site.) The next layer of sediment is siliceous turbites, which extends from about 175 m to 444 m. The gradient of the compressional-wave speed for this material as predicted by Hamilton is 0.761/s, which is significantly smaller than that of the pelagic sediment (1.046/s). The speed at the top of this layer is chosen to match the speed at the bottom of the upper layer. This is somewhat arbitrary, but the compressional-wave speed data from the borehole tend to support this approach.

The layer of siliceous turbites is, however, not uniform below about 220 m. The sediments are interspersed with claystone, mudstone, and chert, or, in acoustical terms, reflector layers. The approximate position, thickness, and compressional speed of these layers as determined from the ODP borehole 387 data is indicated in Fig. 11. The remainder of the compressional-wave speed profile is obtained from the ODP data by taking rough averages of the data. The acoustic basement is assumed to start with the limestone and chalk layers that start near 624 m depth.

Bear in mind that the ODP data are taken from a site that is over one hundred and eighty kilometers north of our site. It is, however, the best information available to our knowledge. Moreover, the literature indicates that our site's sediment structure is quite similar to that of borehole 387.

3.9 Shear-Wave Speed Profile Estimate

With the estimation of the compressional-wave speed profile complete, we again turn to Hamilton to assist in the development of the shear-wave speed profile. In his Fig. 11, Hamilton provides a series of relations that compute the shear-wave speed using the compressional-wave speed as an input parameter [15]. Because the relationships change as the compressional-wave speed varies, slight slope variations exist in the shear-speed profile where none exist in the compressional-speed profile. The resulting shear-wave speed profile is shown as the dashed line in Fig. 11. We are unaware of any shear-wave speed measurements made on the Bermuda Rise with which this profile may be compared.

3.10 Density Profile Estimate

Our density profile, which is shown in Fig. 12, is based on estimates from Hamilton (Table 2 in Ref. [26]) and on the data from ODP borehole 387. Only the initial pelagic layer density (0–175 m) is calculated using Hamilton's relations. The density of the remaining layers is estimated by taking rough averages of the ODP borehole data. The averaging is viewed as sufficient since (as pointed out by Hamilton) other researcher's results have indicated that the density gradient is not as significant as the density jumps at layer interfaces.

3.11 Compressional-Wave Attenuation

Our compressional-wave attenuation profile, which is shown as the solid line in Fig. 13, is obtained from the work of Mitchell and Focke [42]. Mitchell and Focke's values are discussed in the recent survey article on attenuation data by Kibblewhite [7]. In his Fig. 8, Kibblewhite compares Mitchell and Focke's data to the estimates obtained by other workers and shows that their estimates are lower than most other measured attenuation data. The use of the Mitchell and Focke's data on the Bermuda Rise is, however, supported by the work of Frisk *et al.* [3]. If Mitchell and Focke's data are averaged over the upper 160 m, they yield approximately the same value as that cited by Frisk *et al.*, who give an average attenuation estimate for the upper 160 m of sediment at their site on the Bermuda Rise.

A three linear segment approximation to the low attenuation profile that is shown in Mitchell and Focke's Fig. 11 is used. Our attenuation estimates for the sediment layers are shown in Fig. 13 and are based on the Mitchell and Focke's data for the sediment depths indicated. On the other hand, the attenuation estimates of the hard reflector layers are set to the lower attenuation value associated with the deep layers in Mitchell and Focke's data.

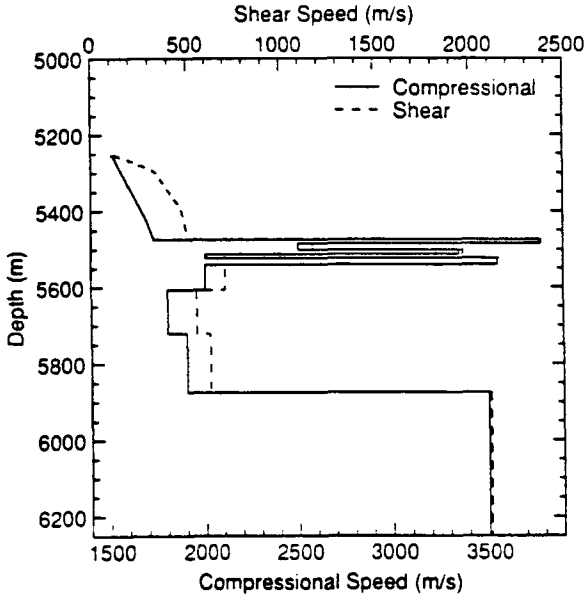

Figure 11: *The compressional-wave speed profile (solid) is developed using gradient estimates from Hamilton and data taken from ODP borehole 387, whereas the shear-wave speed profile (dashed) is developed using estimates of the compressional-wave speed as input to relations provided by Hamilton.*

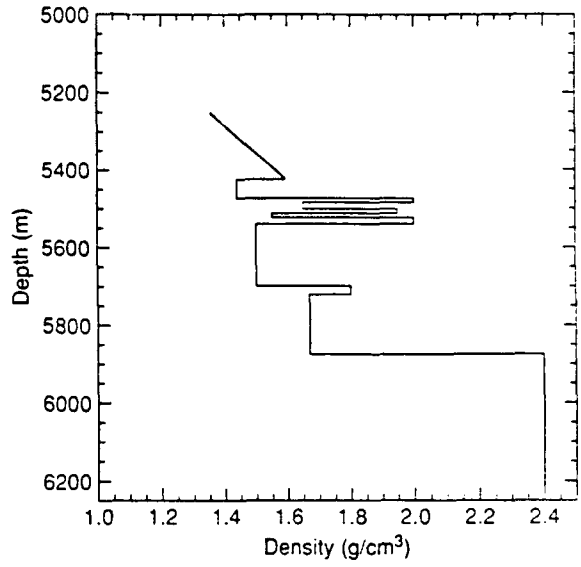

Figure 12: *The density profile is developed using gradient estimates from Hamilton and data taken from ODP borehole 387*

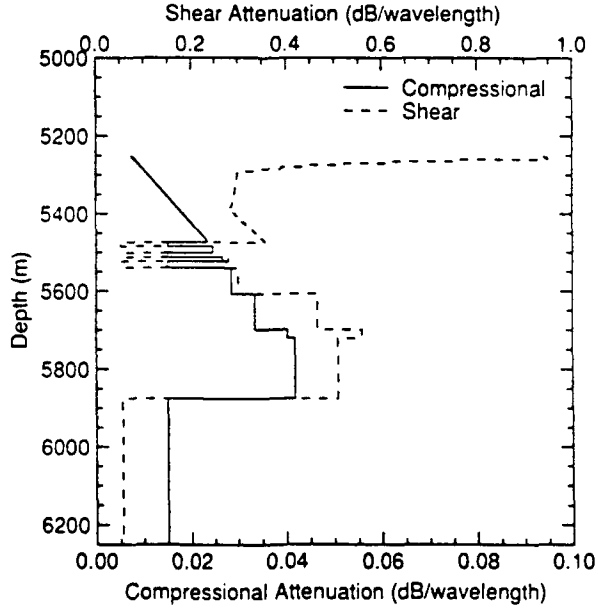

Figure 13: *The compressional-wave attenuation profile (solid) is developed using the data of Mitchell and Focke, whereas the shear-wave attenuation profile (dashed) is chosen to meet the criterion that dilation of the material not radiate energy.*

3.12 Shear-Wave Attenuation

The following relationship between the compressional- and shear-wave attenuations and the compressional- and shear-wave speeds must hold if a pure dilatation of a solid does not radiate energy [11]:

$$\frac{\alpha_s}{\alpha_c}\left(\frac{c_s}{c_c}\right)^2 < \frac{3}{4} \tag{3.1}$$

Because all but the shear-wave attenuation have already been specified, the foregoing relation is used to set an upper bound on the shear-wave attenuation values. In lieu of the upper bound, the shear-wave attenuation is estimated by the procedure set forth by Hamilton: the shear-wave attenuation profile is a scaled version of the compressional-wave attenuation profile, and the scaling factor that is used is 100. The factor of 100 is obtained by comparing the shear- and compressional-wave attenuation plots provided in Figs. 8 and 9 in the article by Kibblewhite [7]. By scaling the compressional-wave attenuation values subject to the upper bound, we obtained the shear-wave attenuation profile that is shown as the dashed line in Fig. 13.

3.13 Epilogue

The geo-acoustic model is now complete and may be used for our reflection- and propagation-loss modelling. The compressional- and shear-wave speed profiles are shown in Fig. 11, the density profile is shown in Fig. 12, and the compressional- and shear-wave attenuation profiles are shown in Fig. 13.

4 Overview of the Propagation- and Reflection-Loss Results

In this section the questions that were posed earlier are revisited, namely, are shear-wave effects important to propagation-loss calculations in this deep-water case, and how much detail in the geo-acoustic model is sufficient? After addressing these questions, we attempt to quantify the effects of modifying some of the parameters in the geo-acoustic model.

4.1 Shear Wave Coupling in the Reflector Layers

To demonstrate the importance of (1) accounting for shear waves in the sea-bed and (2) having a detailed model of the deeper layers, we compare SAFARI's reflection- and propagation-loss predictions for the following scenarios:

1. detailed geo-acoustic model as shown in Figs. 11–13 *with* shear effects,
2. detailed geo-acoustic model *without* shear effects, that is, assume a fluid sub-bottom only,
3. simplified geo-acoustic model as shown in Figs. 14–16 with shear effects,
4. simplified version of the geo-acoustic model without shear effects.

The simplified geo-acoustic model is similar in concept to that used by Frisk *et al.* for their 220 Hz modelling work [3]. The upper unconsolidated sediment is assumed to overlay a homogeneous, harder, faster half-space.

For each of the four scenarios, the reflection loss is calculated as a function of grazing angle for 1–100 Hz, and the propagation loss is calculated at 10 and 20 Hz for different source-receiver geometries. Examination of the reflection-loss output enables us to study the effects of including shear waves and detailed sub-bottom layering in isolation from other propagation effects such as sub-bottom refraction, surface interference, and convergence zones. However, to keep the influence of reflection loss in perspective, we also examine the effect of shear waves and detailed sub-bottom layering on the propagation loss.

Our reflection-loss results, which are generated in the form of grey-scale plots of frequency versus grazing angle, are shown in Figs. 17–20. An examination of the plots indicates that the four different scenarios give very different results. By comparing the reflection-loss results from the simple fluid geo-acoustic model with those from the detailed one (Fig. 17 with Fig. 18), we may make some qualitative statements about the effects of the increased number of sub-bottom layers. In Fig. 17, we see that the angle of incidence at which the reflection loss becomes measurable is approximately constant with frequency, whereas a more complicated pattern is seen in Fig. 18. In the latter, the variations with frequency in the 70–90° range are more sharply defined. The more interesting difference is in the 30–70° region where the reflection loss is exhibiting a frequency-dependent effect that is absent in Fig. 17. Measurable reflection loss is occurring at lower grazing angles for lower frequencies. In concept, the individual layers in the detailed geo-acoustic model are acting similarly to a plate or wall: they selectively permit some frequency and grazing angle combinations to pass with little attenuation, whereas others are totally reflected.

The reflection-loss results for the simple fluid and simple solid geo-acoustic models, Fig. 17 and Fig. 19, may be compared to examine the effects of including shear waves. The contrast is quite dramatic, although not that surprising. The inclusion of shear waves has enabled much more energy to penetrate the sea-bed in the lower 40–70° grazing angle region.

An examination of the results of the detailed solid geo-acoustic model in Fig. 20 indicates elements of both of the features discussed above. The inclusion of shear waves has dramatically broadened the range of grazing angles over which energy is transmitted into the sea-bed, and the detailed layering has increased it even further. In conclusion, the reflection-loss plots indicate (1) that shear waves are an important reflection-loss mechanism for this geo-acoustic environment and (2) that the detailed model of the sub-bottom layers leads to more sharply defined variations of reflection loss with frequency.

The effect of shear waves and detailed sub-bottom layers on the propagation-loss predictions at 20 Hz is now examined. Shown in Figs. 21–24 are the propagation-loss predictions for a 20 Hz source at 15.2 m and a receiver at 30.4 m for each of the four scenarios defined above. The importance of shear waves for this frequency and source-receiver geometry may be assessed by comparing the results in the upper two figures with those in the lower two (Figs. 21 and 22 with Figs. 23 and 24). The inclusion of shear waves leads to an approximately 8 dB increase in the propagation-loss prediction across the entire 0–100 km range. Shear waves are clearly playing a major role in this example: they are increasing the propagation loss, presumably by converting

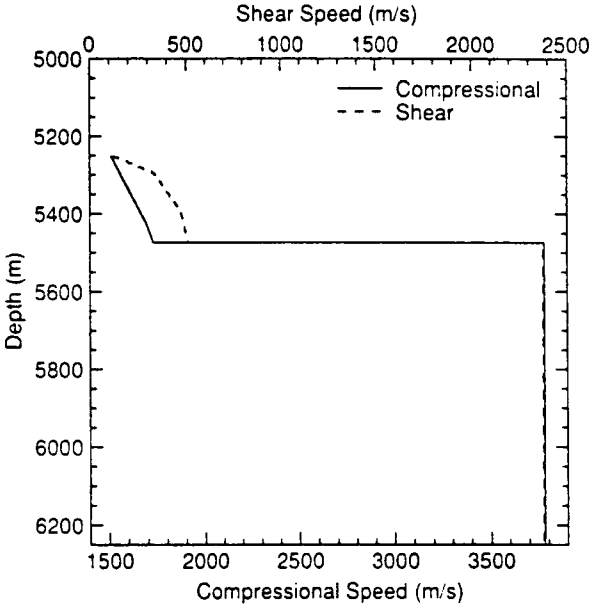

Figure 14: *Simplified forms of the compressional (solid line) and shear (dashed line) speed profiles shown in Fig. 11.*

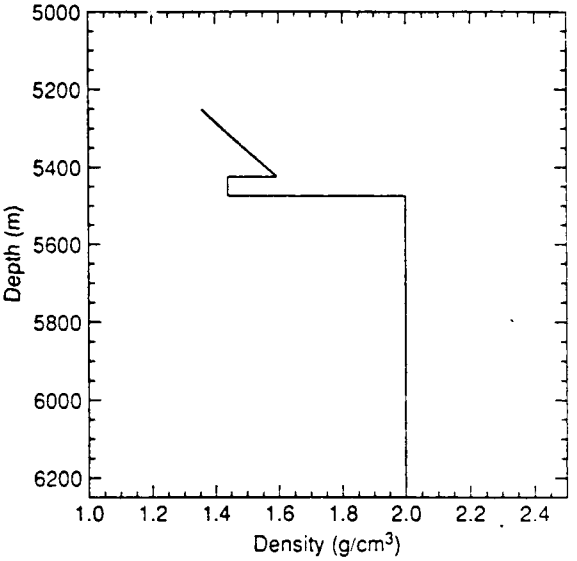

Figure 15: *Simplified form of the density profile shown in Fig. 12.*

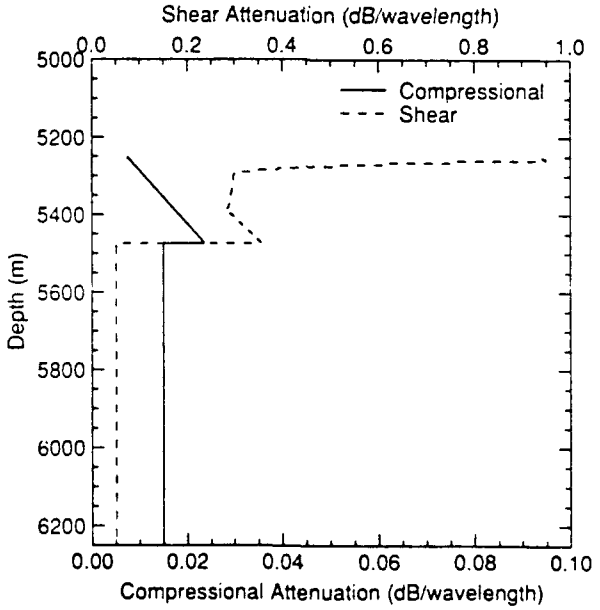

Figure 16: *Simplified forms of the compressional (solid line) and shear (dashed line) attenuation profiles shown in Fig. 13.*

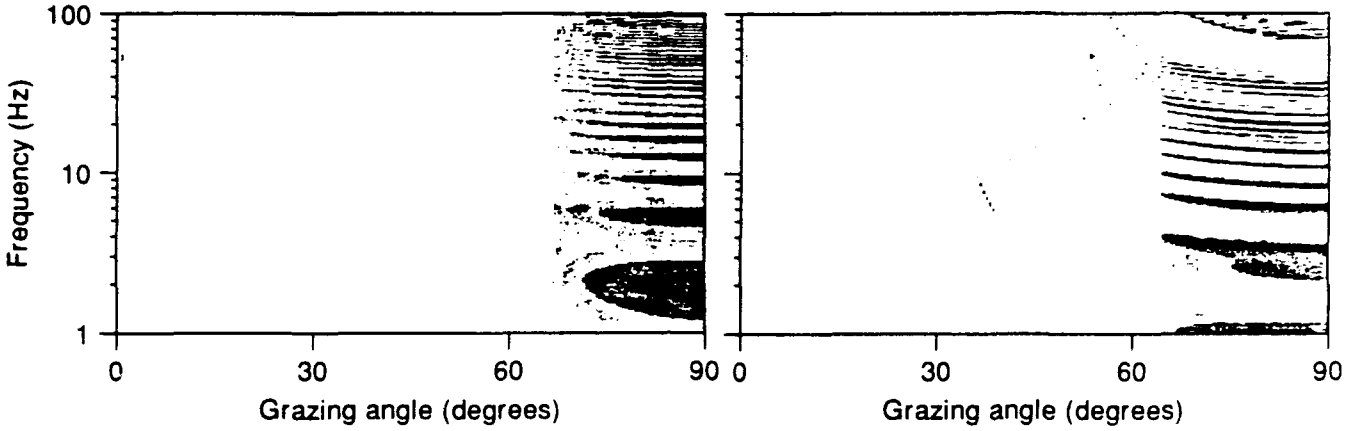

Figure 17: *Grey scale plot of the reflection loss versus frequency and grazing angle for the* simplified *geo-acoustic model* excluding *shear waves.*

Figure 18: *Grey scale plot of the reflection loss versus frequency and grazing angle for the* detailed *geo-acoustic model* excluding *shear waves.*

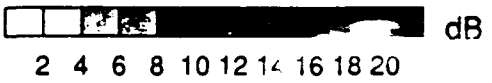

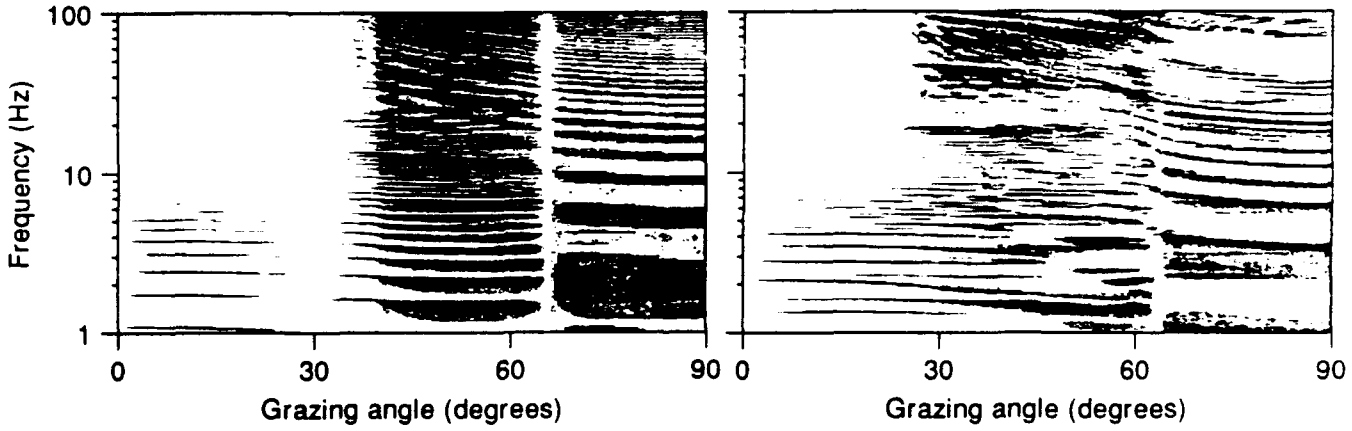

Figure 19: *Grey scale plot of the reflection loss versus frequency and grazing angle for the* simplified *geo-acoustic model* including *shear waves.*

Figure 20: *Grey scale plot of the reflection loss versus frequency and grazing angle for the* detailed *geo-acoustic model* including *shear waves.*

the bottom-interacting compressional waves into shear waves in the bottom.

The importance of detailed sub-bottom layering for this frequency and source-receiver geometry may be assessed by comparing the results in the two figures on the left with those on the right, in particular, Figs. 23 and 24. Detailed sub-bottom layering has led to a difference of about 7 dB at the range of roughly 8 km. Moreover, at ranges greater than 50 km, the rate at which propagation loss increases with range is larger for the detailed sub-bottom case. This leads to about a 5 dB difference in the propagation-loss estimates at 100 km. Thus, for this particular frequency and source-receiver geometry, detailed sub-bottom layering is not as important as accounting for shear waves. It is nevertheless significant if accurate results are required for either short (less than 15 km) or long (greater than 75 km) ranges.

It is important to note that the significance of shear waves and a detailed sub-bottom model varies dramatically with frequency and source-receiver geometry. In the foregoing example, shear waves played a major role, and the detailed sub-bottom model played a lesser but still significant role. Although examples may exist in which shear waves and a detailed sub-bottom model play an even more important role, there are certainly examples in which their role is small. Examine Figs. 25–28, which show the propagation-loss predictions for a 10 Hz source at 91.4 m and a receiver at 304.8 m for each of the four scenarios. It is clear that in this case shear waves and the detailed sub-bottom model have little effect on the propagation-loss results. The primary reason for this dramatic change is the different source-receiver geometry. More energy propagates at angles close the horizontal, and the energy that interacts with the bottom does so at smaller grazing angles. From Figs. 17–20, we see that the reflection loss at small grazing angles is low and independent of shear waves and sub-bottom detail.

4.2 Effects of Varying the Layer Depths

In this section, the effects of varying the depth of the first reflector layer are considered. As a large number of variations are possible in the detailed geo-acoustic model, we do not intend to draw conclusions but merely expose the reader to the issue. Figures 29 and 30 show the reflection-loss grey-scale plots assuming, respectively, that the reflector layer is shallow (150 m) and deep (300 m). The assumed geo-acoustic environment corresponds to the previously discussed simple model including shear waves. For comparison, Fig. 19, shows the corresponding reflection-loss plot for the best-estimate depth (224 m) of the reflector layer. The three graphs show only minor differences in reflection loss with changing reflector depth.

An investigation of the effect of varying the reflector layer depth on the propagation-loss predictions is now conducted by calculating the propagation loss assuming, as above, that the reflector layer is shallow (150 m) and deep (300 m). Figures 31 and 32 show the respective predictions assuming a 10 Hz source at 91.4 m and a receiver at 304.8 m. The differences are the result of the changing reflector depth causing a shift in the interference pattern: for this frequency and source-receiver geometry, the location (in range) of the nulls and peaks is sensitive to the first layer depth. These differences are assumed to be representative of the largest effect caused by the variation in the reflector depth. As an example of a case in which the differences are small, consider Figs. 33 and 34, which show the propagation-loss predictions assuming a 20 Hz source at 15.2 m and a receiver at 30.5 m. Although the shape at short ranges

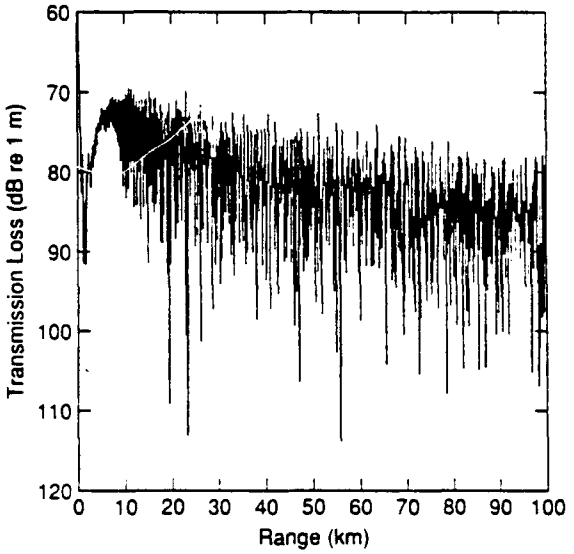

Figure 21: *Propagation loss versus range at 20 Hz with source and receiver depths of 15.2 and 30.5 m, respectively, for the* simplified *geo-acoustic model* excluding *shear waves.*

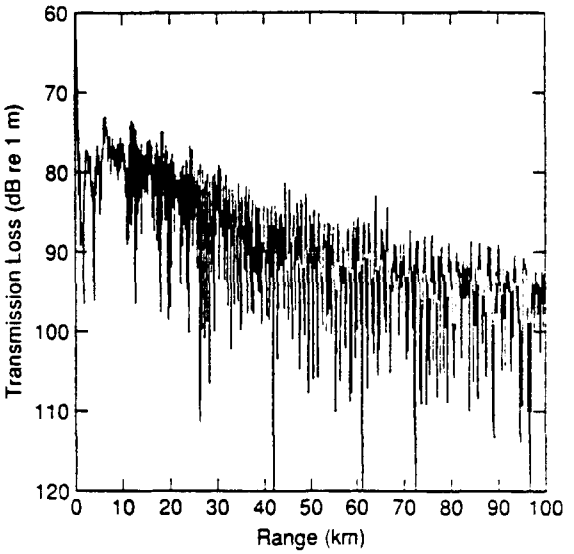

Figure 22: *Propagation loss versus range at 20 Hz with source and receiver depths of 15.2 and 30.5 m, respectively, for the* detailed *geo-acoustic model* excluding *shear waves.*

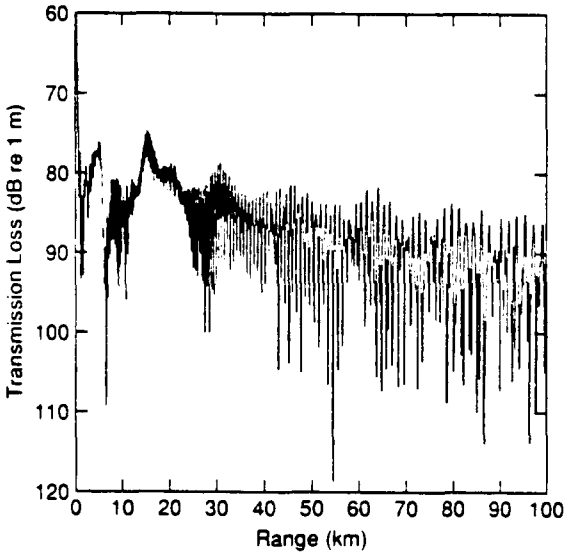

Figure 23: *Propagation loss versus range at 20 Hz with source and receiver depths of 15.2 and 30.5 m, respectively, for the* simplified *geo-acoustic model* including *shear waves.*

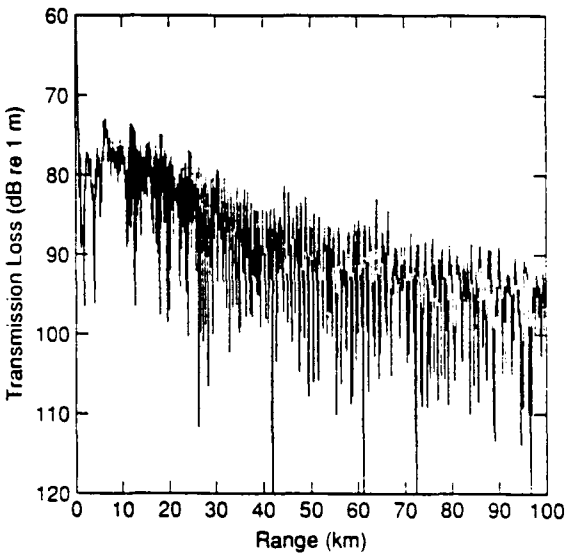

Figure 24: *Propagation loss versus range at 20 Hz with source and receiver depths of 15.2 and 30.5 m, respectively, for the* detailed *geo-acoustic model* including *shear waves.*

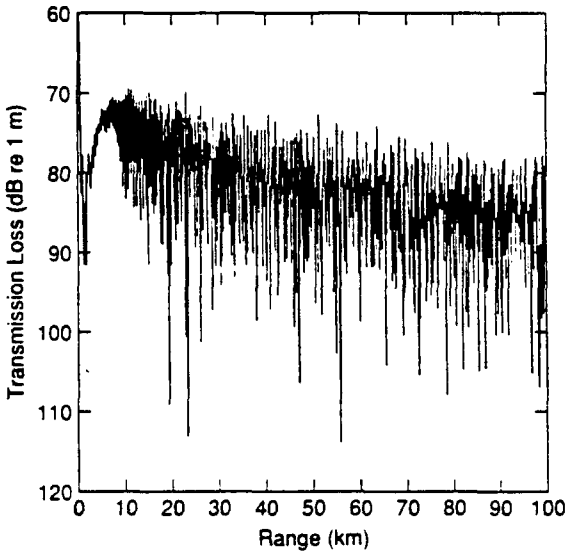

Figure 21: *Propagation loss versus range at 20 Hz with source and receiver depths of 15.2 and 30.5 m, respectively, for the* simplified *geo-acoustic model* excluding *shear waves.*

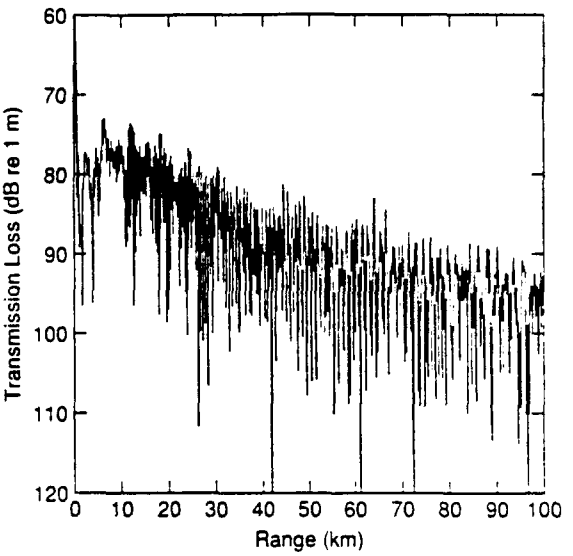

Figure 22: *Propagation loss versus range at 20 Hz with source and receiver depths of 15.2 and 30.5 m, respectively, for the* detailed *geo-acoustic model* excluding *shear waves.*

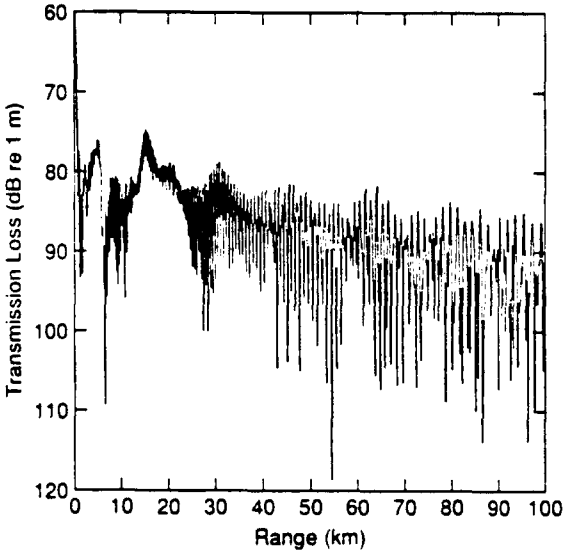

Figure 23: *Propagation loss versus range at 20 Hz with source and receiver depths of 15.2 and 30.5 m, respectively, for the* simplified *geo-acoustic model* including *shear waves.*

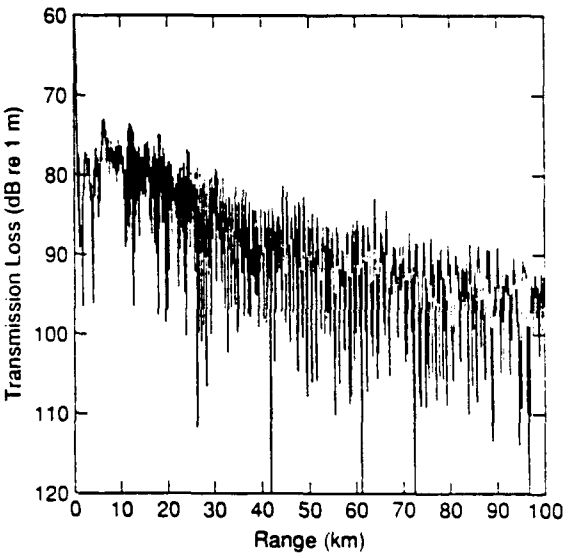

Figure 24: *Propagation loss versus range at 20 Hz with source and receiver depths of 15.2 and 30.5 m, respectively, for the* detailed *geo-acoustic model* including *shear waves.*

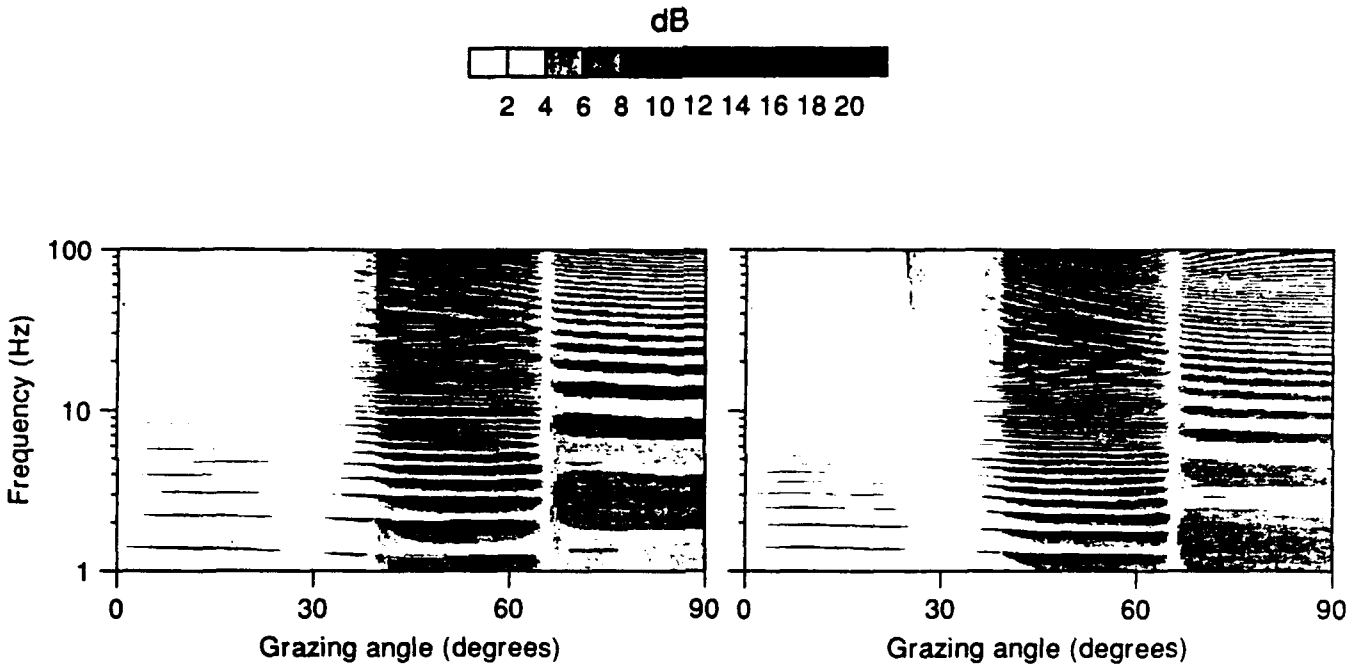

Figure 29: *Grey scale plot of the reflection loss versus frequency and grazing angle for the* simplified *geo-acoustic model(with shallow reflector)* including *shear waves.*

Figure 30: *Grey scale plot of the reflection loss versus frequency and grazing angle for the* simplified *geo-acoustic model(with deep reflector)* including *shear waves.*

appears slightly different, the difference in the average propagation loss is small. Caution must be exercised in generalizing these results, but for the purposes of this memorandum the precise reflector depth is not critical.

5 Acoustic Propagation-Loss Predictions for 5, 10, 20 and 50 Hz

In this section, the acoustic propagation-loss predictions for our site on the Bermuda Rise are presented. For all frequencies, the source depths examined are 15.2 and 91.4 m, whereas the receiver depths examined are 30.5 and 304.8 m. The 5 Hz results are shown in Figs. 35–38, 10 Hz results in Figs. 39–42, 20 Hz results in Figs. 43–46, and 50 Hz results in Figs. 47–50. The geo-acoustic model that is used is the fourth scenario outlined in the previous section, which accounts for shear waves and a detailed sub-bottom layering. The output is now examined for evidence of several other propagation effects: sub-bottom reflections, sub-bottom refraction, surface interference effect, and weakened convergence zones.

The surface interference effect and the weakened convergence zones that occur for shallow, low frequency sources are related effects. The surface interference effect, which is described in detail by Bannister and Pedersen in Ref. [8], is equivalent to saying that a shallow low frequency source acts like a dipole. The majority of the radiated sound energy is directed towards the bottom and propagates to the receiver via bottom-interacting paths. As an example of this effect, examine the 5 Hz propagation-loss curves in Figs. 35–38. The pair of curves with the source at 15.2 m exhibit 10 dB more propagation loss than the corresponding pair with the source at 91.4 m.

Since, for shallow, low frequency sources, less sound energy leaves the source at angles near the horizontal, the energy at the convergence zone is decreased. For our sound-speed profile, the first convergence zone is at a range of approximately 66 km and may be seen fairly easily in the 50 Hz propagation-loss curves for the receiver depth of 30.5 m, Figs. 47 and 49. When the receiver depth is 304.8 m (Figs. 48 and 50), the convergence zone return, which is still easily seen, is split because the receiver responds to the upward and downward refracting energy. As the frequency decreases, so does the energy in the convergence zone returns, and this may be seen by comparing the 50 Hz results with those at 20, 10 and 5 Hz. For the 20 Hz source, the convergence zone return is still noticeable, but for the 10 and 5 Hz sources, the convergence zones are difficult to identify.

We now look for evidence of the sub-bottom reflected paths in the propagation-loss curves. A simplistic model is employed to see if the reflected paths are afforded primarily by the first of the series of sub-bottom reflector layers. A homogeneous ocean (rays are straight lines) is assumed, and the water depth is set to the depth of the top of the first reflector layer. When a 10 Hz source is assumed to be at 91.4 m and a receiver at 304.8 m, the propagation-loss curve obtained is that shown as the solid line in Fig. 51. Shown in the figure as the dashed and/or dotted lines are the individual contributions of the surface-reflector ray pair (Lloyd's mirror pair) and the sets of four rays that compose the first, second, and third bottom-reflected paths. (The propagation-loss curve is the coherent summation of the individual components up to the fifth bottom interaction.) This curve is to be contrasted with the corresponding propagation-loss

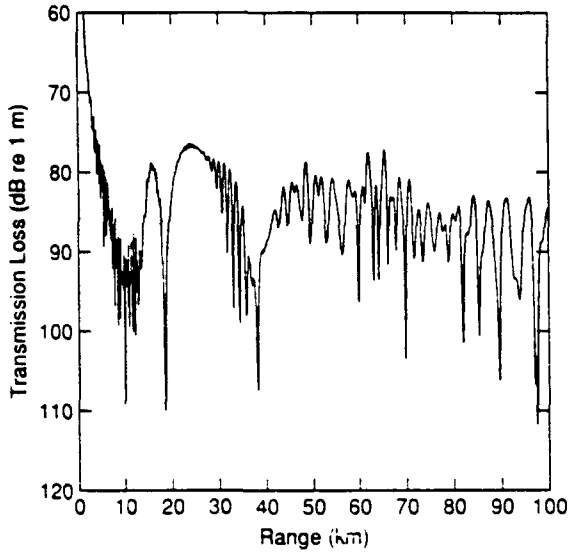

Figure 31: *Propagation loss versus range at 10 Hz with source and receiver depths of 91.4 and 304.8 m, respectively, for the* simplified *geo-acoustic model (with shallower reflector layer)* including *shear waves.*

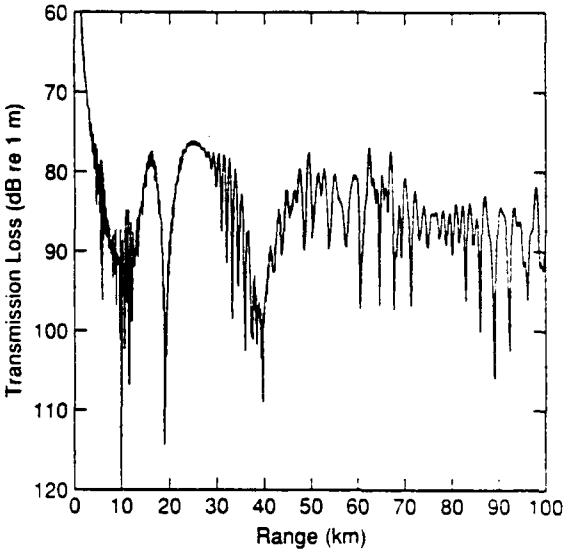

Figure 32: *Propagation loss versus range at 10 Hz with source and receiver depths of 91.4 and 304.8 m, respectively, for the* simplified *geo-acoustic model (with deeper reflector layer)* including *shear waves.*

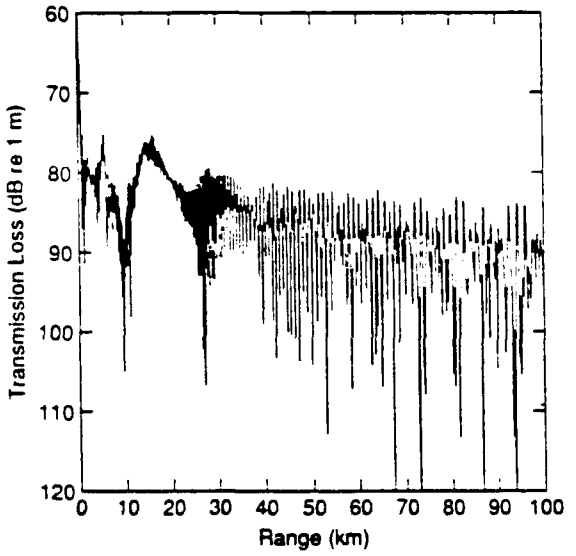

Figure 33: *Propagation loss versus range at 20 Hz with source and receiver depths of 15.2 and 30.5 m, respectively, for the* simplified *geo-acoustic model (with shallower reflector layer)* including *shear waves.*

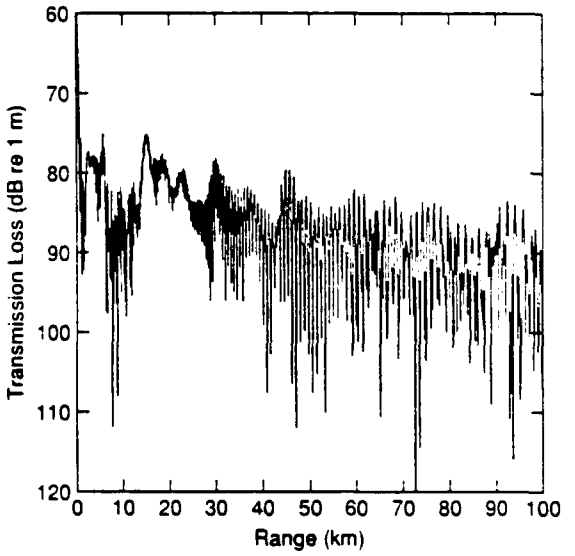

Figure 34: *Propagation loss versus range at 20 Hz with source and receiver depths of 15.2 and 30.5 m, respectively, for the* simplified *geo-acoustic model (with deeper reflector layer)* including *shear waves.*

prediction from SAFARI, which is shown in Fig. 42. Admittedly, the agreement between the two results are perhaps the best of the test cases examined, but it nevertheless indicates the importance of sub-bottom reflected paths in some situations.

Evidence of sub-bottom refraction is difficult to find in this environment. A ray trace diagram for the 91.4 m source is shown in Fig. 52, which is obtained by assuming the upper unconsolidated layer to be part of the water column. In the figure, we see that the first refracted ray reaches the surface between 20 and 21 km in range. Evidence of a decrease in the propagation loss starting at this range is difficult to see in the results, Figs. 35—50. It is possible that the decrease in propagation loss in the 20–30 km range in the 50 Hz results, Figs. 49 and 50, is associated with sub-bottom refraction. However, the number and complexity of the sub-bottom reflection paths makes it difficult to reach conclusions.

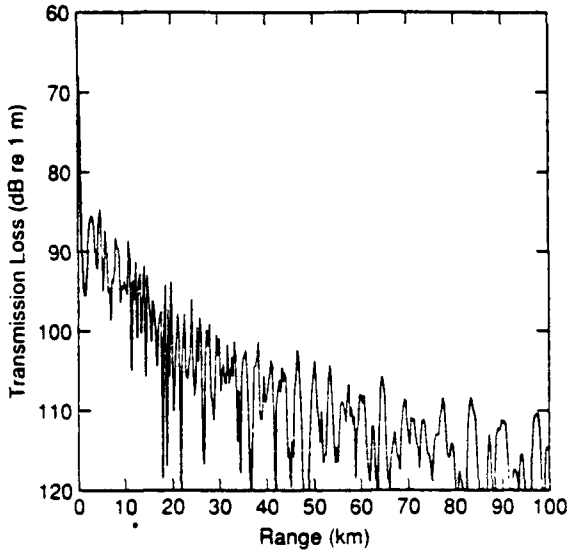

Figure 35: *Propagation loss versus range at 5 Hz with source and receiver depths of 15.2 and 30.5 m, respectively.*

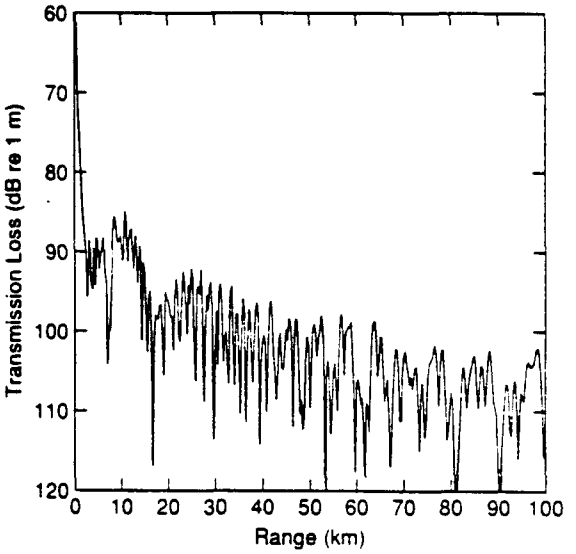

Figure 36: *Propagation loss versus range at 5 Hz with source and receiver depths of 15.2 and 304.8 m, respectively.*

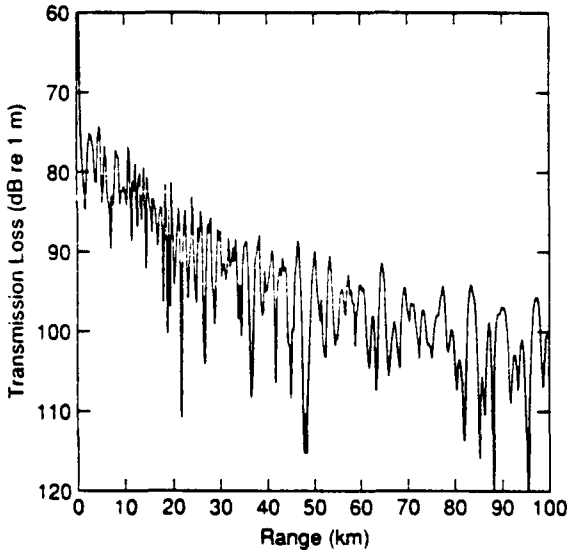

Figure 37: *Propagation loss versus range at 5 Hz with source and receiver depths of 91.4 and 30.5 m, respectively.*

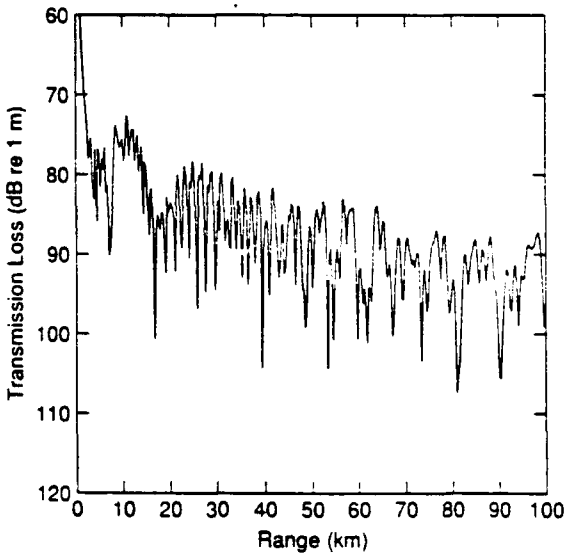

Figure 38: *Propagation loss versus range at 5 Hz with source and receiver depths of 91.4 and 304.8 m, respectively.*

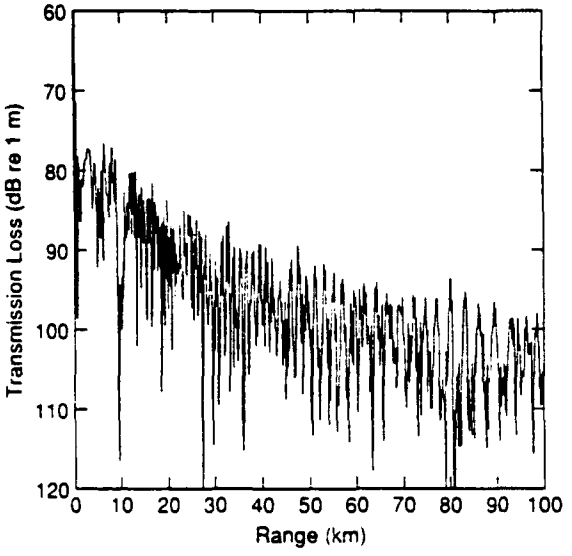

Figure 39: *Propagation loss versus range at 10 Hz with source and receiver depths of 15.2 and 30.5 m, respectively.*

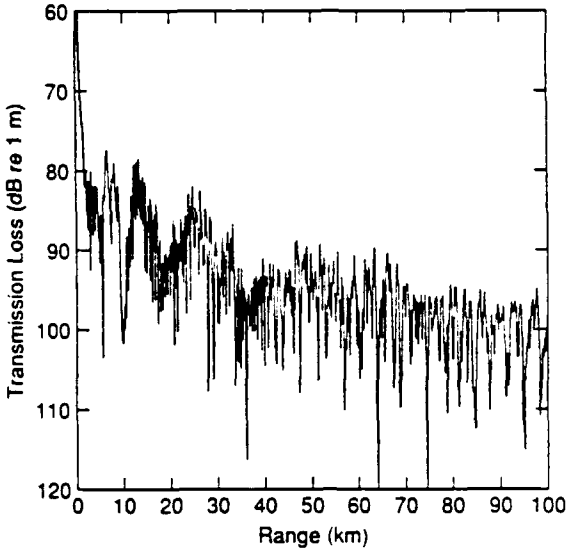

Figure 40: *Propagation loss versus range at 10 Hz with source and receiver depths of 15.2 and 304.8 m, respectively.*

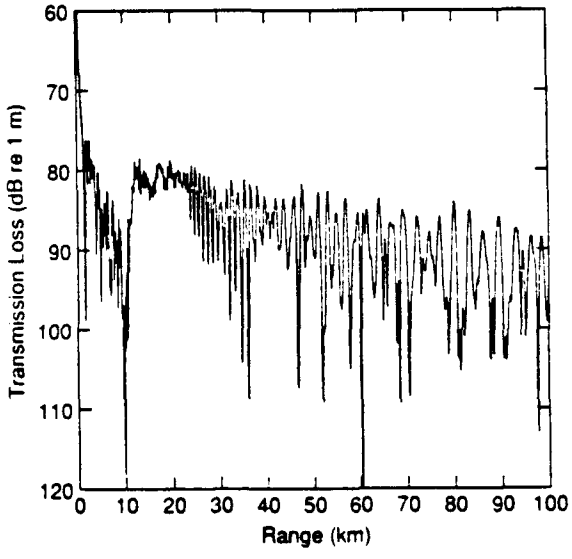

Figure 41: *Propagation loss versus range at 10 Hz with source and receiver depths of 91.4 and 30.5 m, respectively.*

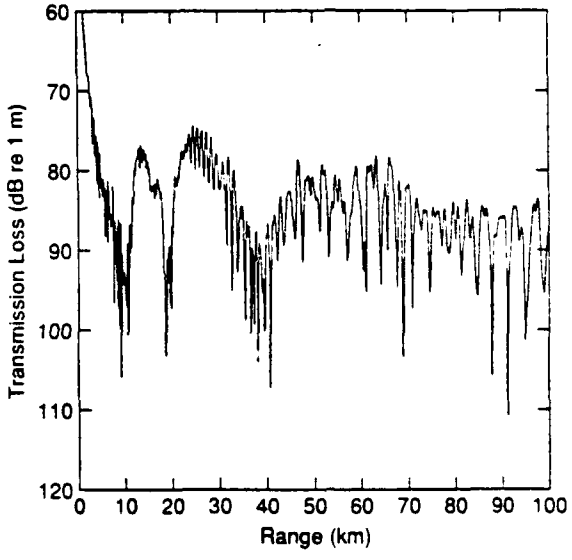

Figure 42: *Propagation loss versus range at 10 Hz with source and receiver depths of 91.4 and 304.8 m, respectively. (Same as Fig. 28).*

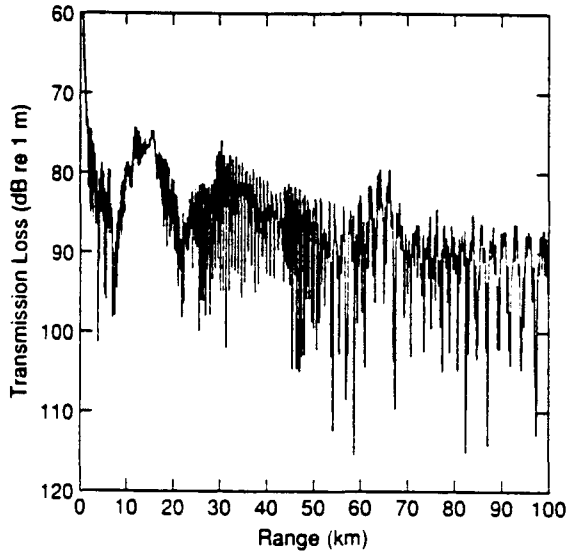

Figure 43: *Propagation loss versus range at 20 Hz with source and receiver depths of 15.2 and 30.5 m, respectively. (Same as Fig. 24).*

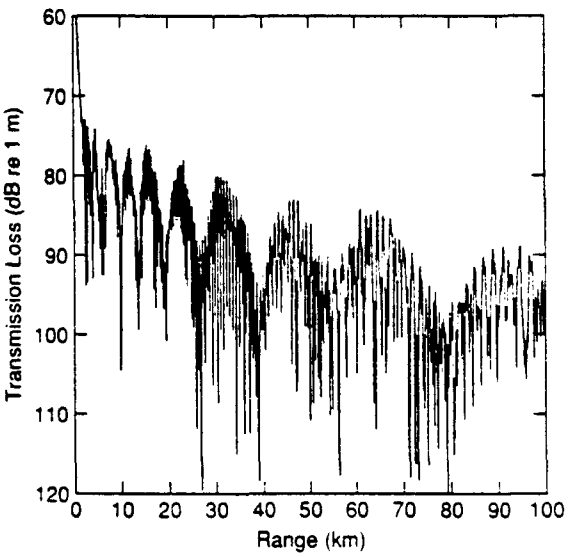

Figure 44: *Propagation loss versus range at 20 Hz with source and receiver depths of 15.2 and 304.8 m, respectively.*

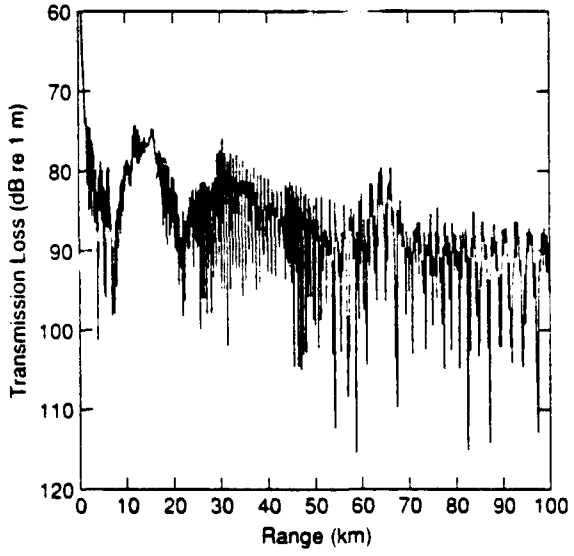

Figure 45: *Propagation loss versus range at 20 Hz with source and receiver depths of 91.4 and 30.5 m, respectively.*

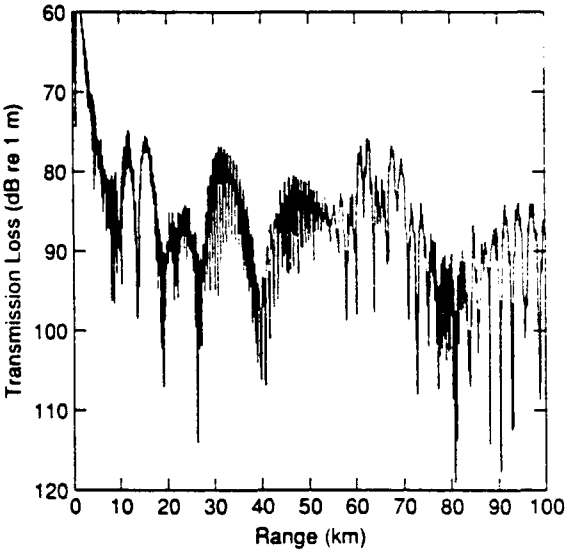

Figure 46: *Propagation loss versus range at 20 Hz with source and receiver depths of 91.4 and 304.8 m, respectively.*

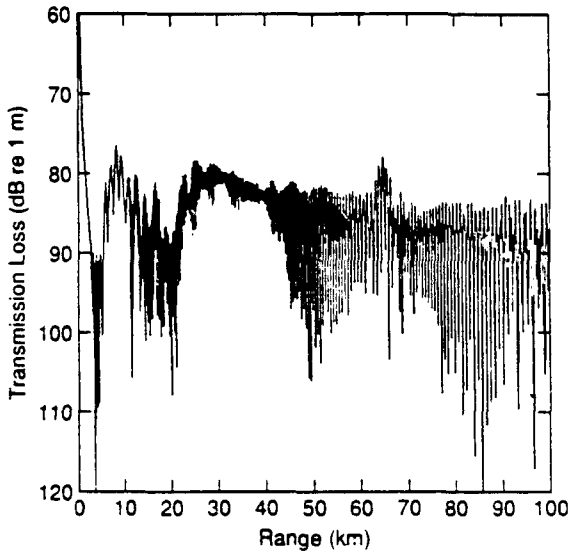

Figure 47: *Propagation loss versus range at 50 Hz with source and receiver depths of 15.2 and 30.5 m, respectively.*

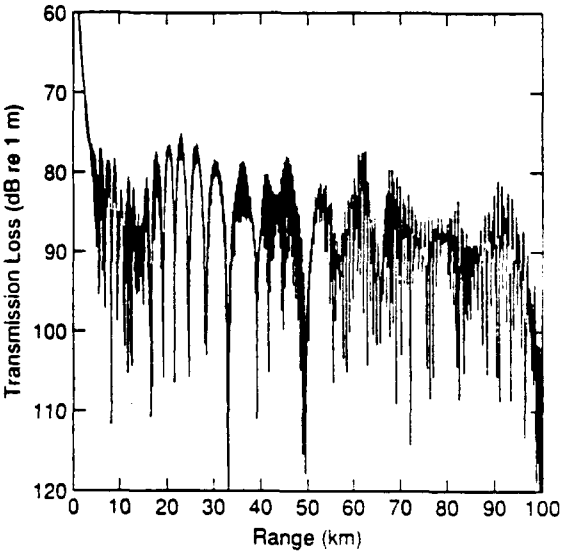

Figure 48: *Propagation loss versus range at 50 Hz with source and receiver depths of 15.2 and 304.8 m, respectively.*

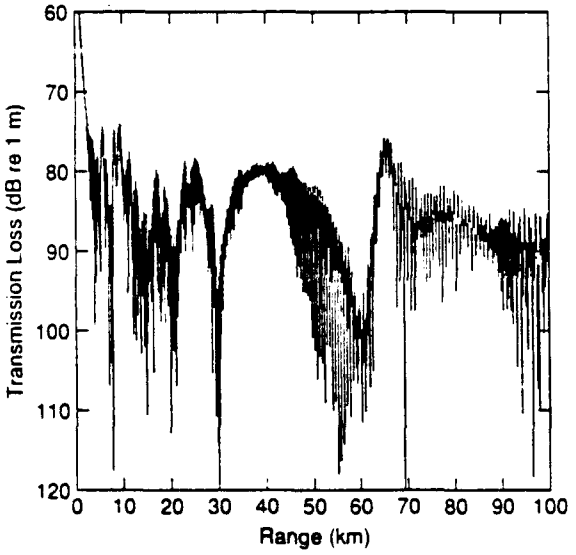

Figure 49: *Propagation loss versus range at 50 Hz with source and receiver depths of 91.4 and 30.5 m, respectively.*

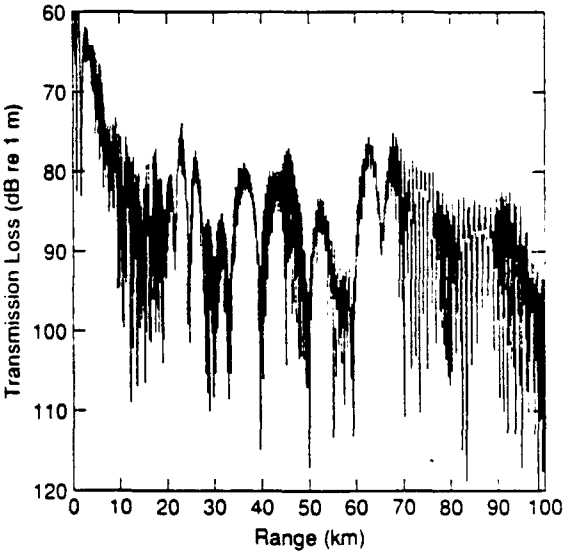

Figure 50: *Propagation loss versus range at 50 Hz with source and receiver depths of 91.4 and 304.8 m, respectively.*

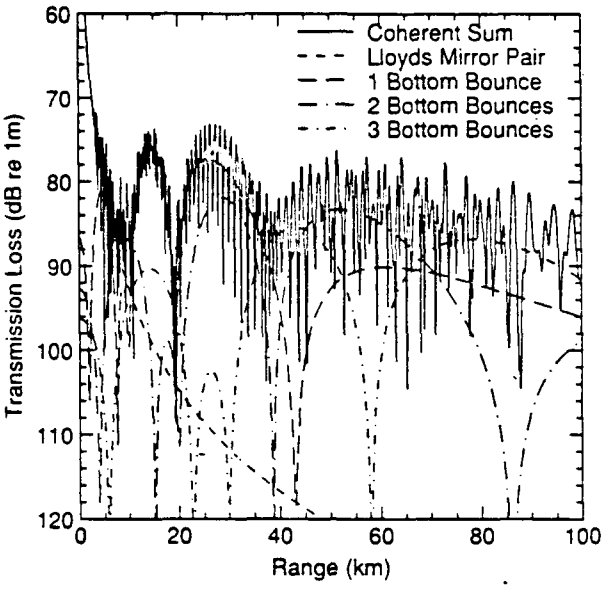

Figure 51: *Propagation loss curve for a 10 Hz source at 91.4 m and a receiver depth of 304.8 m obtained assuming a homogeneous ocean and a water depth of 5470 m (until the top of the first reflector layer).*

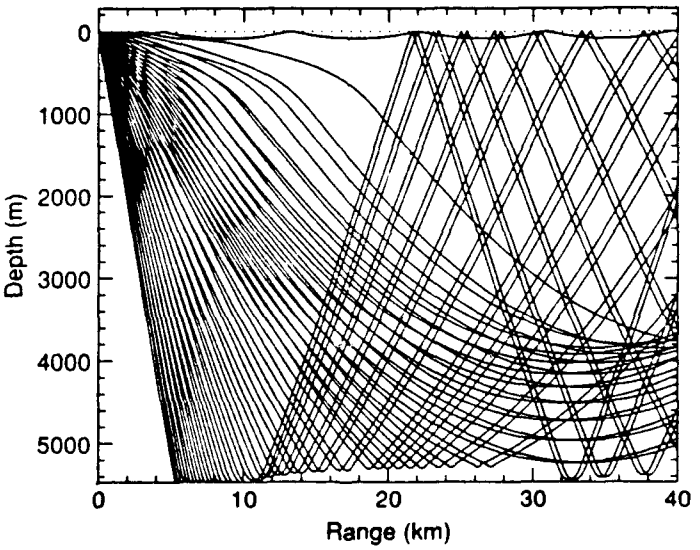

Figure 52: *Ray diagram for the 91.4 m source. The compressional sound-speed profile of the upper unconsolidated layer of sediment is included as part of the water column. Rays are terminated if they strike the "bottom," which is now the top of the first reflector layer at 5470 m.*

6 Summary

In this document, a geo-acoustic model was developed for a site that is on the southwestern part of the Bermuda Rise, a 180 km circle centred at 30°N 69°W. The model was based on an extensive survey of the literature on the geo-acoustic properties of the Bermuda Rise. All available data were compared to obtain the property estimates. The resulting geo-acoustic model gives the compressional- and shear-wave speed profiles, the density profile, and the compressional- and shear-wave attenuation profiles. The profiles extend over 1 km into the sea-bed and are shown in Figs. 11, 12, and 13, respectively.

The geo-acoustic model was used as input to the acoustic propagation-loss model SAFARI, and predictions of the acoustic propagation loss at 5, 10, 20, and 50 Hz for sources at 15.2 and 91.4 m and receivers at 30.5 and 304.8 m were obtained. These results are plotted in Figs. 35–50. Also obtained were predictions of the acoustic reflection loss as a function of frequency and grazing angle; these results were generated in the form of a grey-scale plot of frequency versus grazing angle and are shown in Fig. 20. No comparison with measured acoustic data was attempted. Experiments are required to gather data against which the geo-acoustic model developed in this document could be tested.

The role of shear-wave propagation in the sea-bed was investigated numerically by comparing the reflection- and propagation-loss predictions generated when including shear waves with those generated when excluding shear waves. At the same time, the utility of having a detailed model of the sub-bottom was also investigated numerically by comparing the predictions using our geo-acoustic model with those generated using a simplified version of our model. The simplified version consists of 220 m of unconsolidated sediments overlaying a homogeneous harder, faster half-space. The motivation for the simplified model was that a similar model has been successfully used to model acoustic propagation at 220 Hz for a different location on the Bermuda Rise.

The main result of the numerical investigations was that one cannot assume *a priori* that shear waves and detailed sub-bottom modelling are not required to model low-frequency propagation. Their influence depends on the frequency and source-receiver geometry of the case under investigation. For example, it was noted that if a 20 Hz source was at 15.2 m and a receiver was at 30.4 m, shear waves played a major role in low-frequency propagation, whereas the detailed model of the sub-bottom played a lesser but still significant role. However, if a 10 Hz source was at 91.4 m and a receiver was at 304.8 m, neither shear waves nor detailed sub-bottom information influenced the propagation-loss results.

The effect of small variations in the depth of the upper-most reflective layer was briefly investigated. For the case of a 20 Hz source at 15.2 m and a receiver at 30.4 m, it was noted that the precise depth of the this layer did not significantly affect the propagation-loss results. However, in the case of a 10 Hz source at 91.4 m and a receiver at 304.8 m, propagation was dominated by reflections from the upper-most reflective layer, and variations in the depth of this layer were seen to shift the interference pattern in the propagation-loss curve but not significantly alter its level. Although the consequences of small variations in the depth and thickness of other reflective layers were not explored, we do not believe that such variations have a great effect on the propagation-loss results.

As noted above, sub-bottom reflections played an important role in the propagation for some frequencies and source-receiver geometries. The propagation-loss results were also examined for evidence of sub-bottom refraction. However, for the frequencies and source-receiver geometries examined, sub-bottom refraction was not seen.

References

1. **Acoustics and the Ocean Bottom**, II FASE Specialized Conference, edited by A. Lara, C. Ranz and C. Carbo (Consejo Superior de Investigaciones Cientificas, Madrid, 1987).

2. R. E. Christensen, J. A. Frank, and W. H. Geddes, "Low frequency propagation via shallow refracted paths through deep ocean unconsolidated sediments," *J. Acoust. Soc. Am.* **57**, 1421–1426 (1975).

3. G. V. Frisk, J. A. Doutt, and E. E. Hays, "Bottom interaction of low-frequency acoustic signals at small grazing angles in the deep ocean,"*J. Acoust. Soc. Am.* **69**, 84–94 (1981).

4. I. A. Fraser, personal communication.

5. S. J. Hughes, D. D. Ellis, D. M. F. Chapman, and P. R. Staal, "Low-frequency acoustic propagation over hard-rock seabeds covered by a thin layer of elastic-solid sediment," *J. Acoust. Soc. Am.* **88**, 283–297 (1990).

6. W. M. Ewing, W. S. Jardetzky, and F. Press, *Elastic Waves in Layered Media* (McGraw-Hill Book Co., Inc., New York, 1957).

7. A. C. Kibblewhite, "Attenuation of sound in marine sediments: A review with emphasis on new low-frequency data," *J. Acoust. Soc. Am.* **86**, 716–738 (1989).

8. R. W. Bannister and M. A. Pedersen, "Low-frequency surface interference effects in long-range sound propagation," *J. Acoust. Soc. Am.* **69**, 76–83 (1981).

9. Wycove Systems Ltd., "Calculating Shear Wave Losses as a Perturbation of Normal Mode Results," DREA CR/85/420 (1985).

10. M. Porter, "The Kraken normal mode program," SACLANTCEN Memo. 245, SACLANT Undersea Research Centre, Italy (1991).

11. H. Schmidt, "SAFARI: Seismo-Acoustic Fast field Algorithm for Range-Independent environments," SACLANTCEN Rept. 7642, SACLANT Undersea Research Centre, Italy (1988).

12. F. A. Bowles, "Stratigraphy and sedimentation of the Archipelagic Apron and adjoining area southeast of Bermuda," *Marine Geology* **37**, 267–294 (1980).

13. B. C. Heezen, M. Tharp, and M. Ewing, "The floors of the oceans, I. The North Atlantic," Geol. Soc. Am. Special Paper 65 (1959).

14. L. M. Brekhovskikh, *Waves in Layered Media* (Academic Press, Inc., New York, 1980).

15. E. L. Hamilton, "Acoustic properties of sediments," pp. 3–58 in **Acoustics and the Ocean Bottom**, II FASE Specialized Conference, edited by A. Lara, C. Ranz and C. Carbo (Consejo Superior de Investigaciones Cientificas, Madrid, 1987).

16. E. L. Hamilton, "Geo-acoustic modelling of the sea floor," *J. Acoust. Soc. Am.* **68**, 1313–1340 (1980).

17. E. L. Hamilton, "Prediction of deep-sea sediment properties: state of the art," pp. 1–43 in **Deep-Sea Sediment**, Physical and Mechanical Properties, edited by A. L. Inderbitzen, (Plenum Press, New York, 1979).

18. E. L. Hamilton, "Prediction of in-situ acoustic and elastic properties of marine sediments," *Geophysics* **36**, 266–284 (1971).

19. E. L. Hamilton,"Sound velocity gradients in marine sediments," *J. Acoust. Soc. Am.* **65**, 909–909–922 (1979).

20. E. L. Hamilton, "Sound velocity as a function of depth in marine sediments," *J. Acoust. Soc. Am.* **78**, 1348–1355 (1985).

21. E. L. Hamilton, "Shear wave velocity versus depth in marine sediments: a review," *Geophysics* **41**, 985–996 (1976).

22. E. L. Hamilton, "V_p/V_s and poisson ratios in marine sediments and rocks," *J. Acoust. Soc. Am.* **66**, 1093–1101 (1979).

23. E. L. Hamilton, "Compressional wave attenuation in marine sediments," *Geophysics* **37**, 620–646 (1972).

24. E. L. Hamilton, "Sound attenuation as a function of depth in the sea floor," *J. Acoust. Soc. Am.* **59**, 528–535 (1976).

25. E. L. Hamilton, "Attenuation of shear waves in marine sediments," *J. Acoust. Soc. Am.* **60**, 334–338 (1976).

26. E. L. Hamilton, "Variation of density and porosity with depth in deep-sea sediments," *J. Sed. Petro.* **46**, 280–300 (1976).

27. E L. Hamilton, "Sound velocity-density relations in sea floor sediments and rocks," *J. Acoust. Soc. Am.* **63**, 366–377 (1978).

28. A. J. Silva, E. P. Laine, J. Lipkin, G. R. Heath, and S. A. Akers, "Geotechnical properties of sediments from North Pacific and Northern Bermuda Rise," Tech. Rept. SAND–80–2035C (Sandia National Laboratories, Albuquerque, NM, USA).

29. R. W. Embly, P. J. Hoose, P. Lonsdale, L. Mayer, and B. E. Tucholke, "Furrowed mud waves on the western Bermuda Rise," *Geo. Soc. Am. Bull.* **91**, 731–740 (1980).

30. B. E. Tucholke, "Relationships between the acoustic stratigraphy and lithostratigraphy in the western North Atlantic Basin," Chapter 41 in *Initial Reports of the Deep Sea Drilling Project* **43** (US Government Printing Office, Washington, 1979).

31. B. E. Tucholke, "Structure of basement and distribution of sediments in the western North Atlantic Ocean," Chap. 20 in **The Geology of North America**, Volume M, The Western North Atlantic Region, edited by P. R. Vogt and B. E. Tucholke (The Geological Society of America, 1986).

32. B. A. Trenholm and D. A. Caldwell, "User's Guide to the DREA ICAPS (Integrated Carrier Acoustic Prediction System) Package: A Subset of the US Navy ICAPS Package," Vol. I (User's Guide) and Vol. II (Program Listings), DREA RN/AM/80/3, Informal Communication (1980) (Restricted).

33. E. M. Podeszwa, "Sound speed profiles for the North Atlantic Ocean," NUSC Tech. Doc. 5447 (Naval Underwater Systems Center, Newport, RI, 1979).

34. M. Ewing, J. L. Worzel, *et al.*, "Site 7," Chapter 7 in *Initial Reports of the Deep Sea Drilling Project* **1** (US Government Printing Office, Washington, 1969).

35. M. Ewing, J. L. Worzel, *et al.*, "Site 6," Chapter 6 in *Initial Reports of the Deep Sea Drilling Project* **1** (US Government Printing Office, Washington, 1969).

36. G. F. Gettrust, M. Grimm, S. Madosik, and M. Rowe, "Results of a deep-tow multichannel survey on the Bermuda Rise," *Geophys. Res. Let.* **15**, 1413-1416 (1988).

37. R. E. Houtz, "Comparison of velocity-depth characteristics in western North Atlantic and Norwegian Sea sediments," *J. Acoust. Soc. Am.* **68**, 1409-1414 (1980).

38. K. O. Emery, E. Uchupi, J. D. Phillips, C. O. Bowin, E. T. Bunce, and S. T. Knott, "Continental Rise off Eastern North America," *Am. Assoc. Petro. Geol. Bull.* **54**, 44-108 (1970).

39. R. E. Houtz and J. I. Ewing, "Detailed Sedimentary Velocities from Seismic Refraction Profiles in the Western North Atlantic," *J. Geophys. Res.* **68**, 5233-5358 (1963).

40. M. Ewing and J. Ewing, "Sediments at proposed LOCO drilling sites," *J. Geophys. Res.* **68**, 251-256 (1963).

41. B. E. Tucholke, P. R. Vogt, *et al.*, "Site 387: Cretaceous to Recent Sedimentary Evolution of the Western Bermuda Rise," Chapter 6 in *Initial Reports of the Deep Sea Drilling Project* **43** (US Government Printing Office, Washington, 1979).

42. S. K. Mitchell and K. C. Focke, "New measurements of compressional wave attenuation in deep ocean sediments," *J. Acoust. Soc. Am.* **67**, 1582-1589 (1980).

DOCUMENT CONTROL DATA

(Security classification of title, body of abstract and indexing annotation must be entered when the overall document is classified)

1. ORIGINATOR (The name and address of the organization preparing the document. Organizations for whom the document was prepared, e.g. Establishment sponsoring a contractor's report, or tasking agency, are entered in section 8.)

Defence Research Establishment Atlantic
P.O. Box 1012, Dartmouth, N.S. B2Y 3Z7

2. SECURITY CLASSIFICATION (Overall security of the document including special warning terms if applicable.)

Unclassified

3. TITLE (The complete document title as indicated on the title page. Its classification should be indicated by the appropriate abbreviation (S,C,R or U) in parentheses after the title.)

Acoustic Propagation Loss Predictions for a Site on the Bermuda Rise at Low and Very Low Frequencies

4. AUTHORS (Last name, first name, middle initial. If military, show rank, e.g. Doe, Maj. John E.)

Cotaras, Frederick D. and Theriault, James A.

5. DATE OF PUBLICATION (Month and year of publication of document.)

June 1992

6a. NO. OF PAGES (Total containing information. Include Annexes, Appendices, etc.)

44

6b. NO. OF REFS. (Total cited in document.)

42

6. DESCRIPTIVE NOTES (The category of the document, e.g. technical report, technical note or memorandum. If appropriate, enter the type of report, e.g. interim, progress, summary, annual or final. Give the inclusive dates when a specific reporting period is covered.)

Technical Memorandum

8. SPONSORING ACTIVITY (The name of the department project office or laboratory sponsoring the reseach and development. Include the address.)

Defence Research Establishment Atlantic
P.O. Box 1012, Dartmouth, N.S. B2Y 3Z7

9a. PROJECT OR GRANT NUMBER (If appropriate, the applicable research and development project or grant number under which the document was written. Please specify whether project or grant.)

2AA-19

9b. CONTRACT NUMBER (If appropriate, the applicable number under which the document was written.)

10a. ORIGINATOR'S DOCUMENT NUMBER (The official document number by which the document is identified by the originating activity. This number mrst be unique to this document.)

DREA Technical Memorandum 92/215

10b. OTHER DOCUMENT NUMBERS (Any other numbers which may be assigned this document either by the originator or by the sponsor.)

11. DOCUMENT AVAILABILITY (Any limitations on further dissemination of the document, other than those imposed by security classification)

- (X) Unlimited distribution
- ( ) Distribution limited to defence departments and defence contractors; further distribution only as approved
- ( ) Distribution limited to defence departments and Canadian defence contractors; further distribution only as approved
- ( ) Distribution limited to government departments and agencies; futher distribution only as approved
- ( ) Distribution limited to defence departments; further distribution only as approved
- ( ) Other (please specify):

12. DOCUMENT ANNOUNCEMENT (Any limitation to the bibliographic annoucement of this document. This will normally correspond to the Document Availability (11). However, where futher distribution (beyond the audience specified in 11) is possible, a wider announcement audience may be selected.)

13. ABSTRACT (A brief and factual summary of the document. It may also appear elsewhere in the body of the document itself. It is highly desirable that the abstract of classified documents be unclassified. Each paragraph of the abstract shall begin with an indication of the security classification of the information in the paragraph (unless the document itself is unclassified) represented as (S), (C), (R), or (U). It is not necessary to include here abstracts in both offical languages unless the text is bilingual)

Low (10 -100 Hz) and very low (1 -10 Hz) frequency acoustic propagation loss is predicted for a site on the Bermuda Rise near 30°N 69°W. An extensive survey of the open literature is reported, and a geo-acoustic model of the acoustic environment at the site is developed. The results of a brief numerical investigation of the effect of shear waves and detailed sub-bottom layering on the acoustic propagation-loss predictions are discussed. The acoustic propagation-loss model used is SAFARI, which accounts for shear waves in the sediment but assumes a range-invariant environment. The propagation-loss predictions for 5, 10, 20, and 50 Hz are then presented. Also presented are predictions of the reflection loss in the form of grey-scale plots as a function of frequency and grazing angle. No comparison with experimental data is attempted.

14. KEYWORDS, DESCRIPTORS or IDENTIFIERS (Technically meaningful terms or short phrases that characterize a document and could be helpful in cataloguing the document. They should be selected so that no security classification is required. Identifiers, such as equipment model designation, trade name, military project code name, geographic location may also be included. If possible keywords should be selected from a published thesaurus. e.g. Thesaurus of Engineering and Scientific Terms (TEST) and that thesaurus-identified. If it is not possible to select indexing terms which are Unclassified, the classification of each should be indicated as with the title.)

propagation-loss
Bermuda Rise
SAFARI
model predictions
very low frequencies
reflection loss
shear waves
geo-acoustic models
underwater acoustics